ACS EARTH AND SPACE CHEMISTRY

http://pubs.acs.org/journal/aesccq

Article

Reaction Mechanisms Underlying Unfunctionalized Alkyl Nitrate Hydrolysis in Aqueous Aerosols

Fatemeh Keshavarz,* Joel A. Thornton, Hanna Vehkamäki, and Theo Kurtén

Cite This: *ACS Earth Space Chem.* 2021, 5, 210–225

Read Online

ACCESS | Metrics & More | Article Recommendations | Supporting Information

ABSTRACT: Alkyl nitrates (ANs) are both sinks and sources of nitrogen oxide radicals (NOx = NO + NO_2) in the atmosphere. Their reactions affect both the nitrogen cycle and ozone formation and therefore air quality and climate. ANs can be emitted to the atmosphere or produced in the gas phase. In either case, they can partition into aqueous aerosols, where they might undergo hydrolysis, producing highly soluble nitrate products, and act as a permanent sink for NOx. The kinetics of AN hydrolysis partly determines the extent of AN contribution to the nitrogen cycle. However, kinetics of many ANs in various aerosols is unknown, and there are conflicting arguments about the effect of acidity and basicity on the hydrolysis process. Using computational methods, this study proposes a mechanism for the reactions of methyl, ethyl, propyl, and butyl nitrates with OH^- (hydroxyl ion; basic hydrolysis), water (neutral hydrolysis), and H_3O^+ (hydronium ion; acidic hydrolysis). Using quantum chemical data and transition state theory, we follow the effect of pH on the contribution of the basic, neutral, and acidic hydrolysis channels, and the rate coefficients of AN hydrolysis over a wide range of pH. Our results show that basic hydrolysis (i.e., AN reaction with OH^-) is the most kinetically and thermodynamically favorable reaction among our evaluated reaction schemes. Furthermore, comparison of our kinetics results with experimental data suggests that there is an as yet unknown acidic mechanism responsible for acidic catalysis of AN hydrolysis.

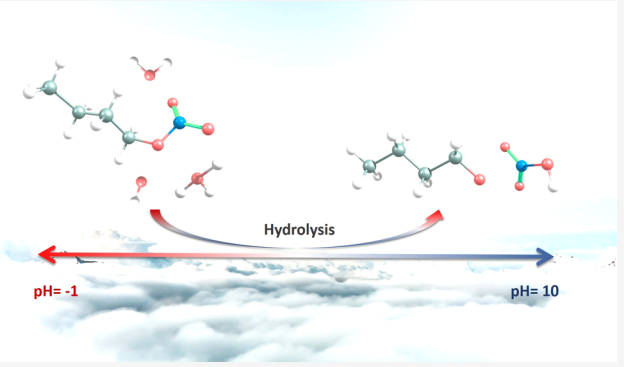

KEYWORDS: *alkyl nitrate, reaction kinetics, acidic hydrolysis, basic hydrolysis, rate coefficient*

INTRODUCTION

The nitrogen cycle is one of the most important chemical cycles in the atmosphere and plays a key role in regional air quality, human health, and climate.[1] The atmospheric component of this cycle starts with nitrogen oxide radicals (NOx = NO + NO_2) that catalyze the generation of tropospheric ozone.[2,3] NOx can be transformed into a diverse set of nitrogen-containing chemical compounds including, but not limited to, nitric acid (HNO_3), nitrous acid (HNO_2), peroxynitric acid ($HOONO_2$), dissolved or solid nitrate (NO_3^-) salts in aerosols, and alkyl nitrates (ANs; $RONO_2$, R = $C_xH_yO_z$).[4]

The main day-time route of AN production from NOx involves oxidation of a parent volatile organic compound (VOC) to form an organic peroxy radical (RO_2), which upon reaction with NO forms either an alkoxy radical (RO) and NO_2 or an alkyl nitrate ($RONO_2$) (see reactions R1–R3b).[4] Generally, the yield and branching ratios of R3a and R3b depend on the nature of the alkyl group, temperature, and pressure. The branching ratio of R3b varies from one to tens of percent, scaling with the number of carbons (and other heavy atoms) in the RO_2.[5] Other, usually minor, channels for AN production also exist. For example, under very polluted conditions, reactions of alkoxy radicals (RO) with NO_2 (R4) can principally lead to ANs. However, the yield of this reaction is limited by the extremely short atmospheric lifetime of RO.[6,7]

$$RH + OH \rightarrow R + H_2O \quad (R1)$$

$$R + O_2 \rightarrow RO_2 \quad (R2)$$

$$RO_2 + NO \rightarrow RO + NO_2 \quad (R3a)$$

$$\rightarrow RONO_2 \quad (R3b)$$

$$RO + NO_2 + M \rightarrow RONO_2 + M \quad (R4)$$

At night, when the concentration of the atmospheric OH radical is low, $RONO_2$ is produced through ozone-based oxidation of NO_2 into NO_3 (R5)[8] and the reaction of NO_3 with tropospheric VOCs (R6).[9] The AN production

Received: September 8, 2020
Revised: December 3, 2020
Accepted: December 15, 2020
Published: January 12, 2021

mechanism typically involves NO_3 addition to a C=C double bond, followed by O_2 addition to generate a nitrooxyperoxy radical. Finally, reactions of the nitrooxyperoxy radicals with either HO_2, RO_2, NO, or NO_3 can produce ANs with various substitutions.[5] This night-time process can result in $RONO_2$ branching ratios as high as 80%.[10] However, it loses its effectiveness during daytime because of fast NO_3 photolysis (R7) and the reaction of NO_3 with NO (R8).[8,11]

$$NO_2 + O_3 \rightarrow NO_3 + O_2 \quad (R5)$$

$$NO_3 + VOC \rightarrow RONO_2 \quad (R6)$$

$$NO_3 + h\nu \rightarrow NO_2 + O \quad (R7a)$$

$$\rightarrow NO + O_2 \quad (R7b)$$

$$NO_3 + NO \rightarrow 2NO_2 \quad (R8)$$

In addition to the outlined methods of AN production, some atmospheric ANs might be directly emitted to the atmosphere from marine sources.[12,13] Particularly, the main source of methyl (Me; CH_3ONO_2) and ethyl (Et; $C_2H_5ONO_2$) nitrates is marine emissions.[14,15] In contrast, most ANs with larger alkyl groups are produced via reactions R1−R7b.[15,16] Finally, anthropogenic activities, such as biomass burning[17] and application of nitrogen-rich and AN explosives,[14] can also load the atmospheric nitrogen cycle with additional ANs.[4]

The ANs can be removed from the atmosphere via several processes including dry deposition (e.g., to forests)[4,8] and uptake of gas-phase ANs by plants.[18] Another removal method is gas-phase oxidation (e.g., R9), which releases NOx back into the atmosphere. Since ANs have relatively long atmospheric lifetimes, they can act as a reservoir and transport NOx to remote regions,[1,19] thus influencing the NOx−O_3−HOx cycle also away from polluted areas.[4] Beside oxidation, ANs can undergo gas-phase photolysis (R11), which recycles NOx, and generally has effects similar to oxidation.[12,20]

The removal of ANs is not limited to the gas phase as they can partition into atmospheric aerosols,[21,22] where they can photolyze into the RO and NO_2 radicals (similar to reaction a) or undergo hydrolysis (e.g., R11−R13).[23−25] Hydrolysis of ANs in the aqueous phase of aerosols alters the chemistry of organic aerosols.[26] It also plays a role in the nitrogen cycle by converting ANs to alcohols and other products.[27] Specifically, although some hydrolysis products, such as alcohols and olefins with high saturation concentration,[28] tend to partition back to the gas phase,[23] some other products, for example, NO_3^- and HNO_3, can completely or partially remain in the aqueous phase.[1,25] In this way, AN hydrolysis perturbs the gas/condensed phase partitioning and potentially increases AN uptake according to the Le Chatelier's principle.[29,30] Simultaneously, the hydrolysis reaction decreases the mass of organic aerosols by consuming their organic nitrate content and producing smaller (more volatile) products.[23,31] Although many studies claim that AN hydrolysis mainly matters under humid conditions, for example, refs,[25,30,32,33] other studies have asserted that the degree of AN partitioning from the gas phase to particles and also their particle-phase hydrolysis can be high even at low relative humidity.[29]

$$RONO_2 + OH \rightarrow ROH + NO_3 \quad (R9)$$

$$RONO_2 + h\nu \rightarrow RO + NO_2 \quad (R10a)$$

$$RONO_2 + h\nu \rightarrow R + NO_3 \quad (R10b)$$

$$RONO_2 + H_2O \rightarrow ROH + HNO_3(aqueous) \quad (R11)$$

$$RONO_2 + OH^- \rightarrow ROH + NO_3^-(aqueous) \quad (R12)$$

$$RONO_2 + H_3O^+ \rightarrow ROH_2^+ + HNO_3(aqueous) \quad (R13)$$

A large number of studies have investigated AN hydrolysis or they have invoked AN uptake and hydrolysis to explain their observations. However, a detailed molecular-level general mechanism for the hydrolysis reaction of AN under different conditions is still missing. Instead, most studies have assumed that AN hydrolysis leads to the production of alcohols and nitric acid. Some studies have also considered that ANs can undergo nucleophilic substitution or hydrogen elimination by hydroxyl anions (OH^-), for example, in refs.[23,34,38] Rindelaub et al.[23] proposed a reaction mechanism for "acid-catalyzed hydrolysis" of several ANs derived from α-pinene by combining experimental evidences and computational methods. Their developed mechanism supported the production of alcohols, alkenes, and nitric acid.

To date, there are a limited number of kinetics studies on AN hydrolysis. One of the best examples of systematic kinetics studies on AN hydrolysis is that of Hu et al.,[27] who studied acidic hydrolysis of a set of mono-and di-functional organosulfates and organonitrates. One deficiency of most kinetics studies to date is that they are typically condition-specific and performed for a limited range of pH, mainly highly acidic or basic conditions. Moreover, there is no agreement about the effect of acidity on AN hydrolysis. Lucas and Hammett[28] concluded that the hydroxyl ion (basicity) increases the rate of AN hydrolysis, whereas "acids have no effect". Also, Gaffney et al.[39] stated that methyl nitrate hydrolysis is negligible in moderately acidic solutions. In contrast, Boschan et al.[36] outlined in their review on the chemistry of ANs that acids can slightly enhance AN hydrolysis, while Hu et al.[27] found that ANs are unstable under the acidic conditions typical of atmospheric aerosols because of hydrolysis and reaction with sulfuric acid. However, they also reported that extremely acidic conditions are necessary to catalyze the reaction and observe efficient hydrolysis of primary and secondary ANs. Rindelaub et al.[1] stated that ANs can readily hydrolyze with rate constants that are positively correlated with acidity, but they also declared that the effect of acidity on hydrolysis of ANs is unknown. In their later studies, they confirmed that the mechanism of AN hydrolysis is "acid-catalyzed", but the exact mechanism is uncertain.[23,29] The conflict between studies claiming acid catalysis and studies finding no evidence for it is also described by Zare et al.[25]

To shed light into the controversial matter, this study focuses on a series of straight chain ANs including methyl (Me), ethyl (Et), propyl (Pr), and butyl (Bu) nitrates, with 1−200 pptv[4,12,13] concentration in the atmosphere (equivalent to 1.95×10^{-12} to 3.90×10^{-10} mol L^{-1} in aqueous aerosols considering the Henry's law coefficients (H) of H_{Me} = 2.64 mol L^{-1} atm^{-1}; H_{Et} = 2.18 mol L^{-1} atm^{-1}; H_{Pr} = 1.55 mol L^{-1} atm^{-1}; and H_{Bu} = 1.44 mol L^{-1} atm^{-1}).[40] In the first step, the mechanism of the AN reaction with water, OH^-, and H_3O^+ is studied to represent neutral, basic, and acidic AN hydrolysis, respectively. We also model the protonation of ANs and the hydrolysis of their protonated form. In the next step, a computational framework is devised to calculate the rate coefficient of AN hydrolysis at a specific pH. Next, our reaction

https://dx.doi.org/10.1021/acsearthspacechem.0c00253
ACS Earth Space Chem. 2021, 5, 210−225

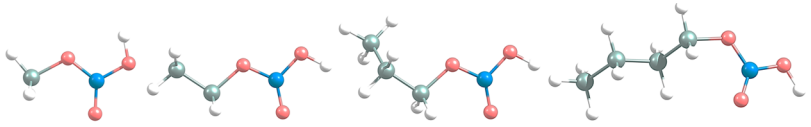

Me: -429.1 (+77.5) Et: -432.6 (+74.0) Pr: -432.7 (+73.9) Bu: -430.4 (+76.2)

Figure 1. The most stable geometry of the protonated methyl (Me), ethyl (Et), propyl (Pr), and butyl (Bu) nitrates. The values under each structure refer to their Gibbs free energy of protonation (298.15 K and 1 atm; in kJ mol^{-1}) calculated at the CCSD(T)/cc-pVDZ//ωB97X-D/def2-TZVP level for the reactions of $H^+(aq) + RONO_2\ (aq) \rightarrow RONO(OH)^+(aq)$ and $H_3O^+\ (aq) + RONO_2\ (aq) \rightarrow H_2O + RONO(OH)^+(aq)$ (in parentheses).

profiles are introduced into the devised framework to calculate the pseudo-first-order and bimolecular rate coefficients of AN hydrolysis over a wide pH range, covering all potential tropospheric conditions. Also, the related half-lives are estimated. Finally, the kinetics results are discussed and compared to the available experimental data.

COMPUTATIONAL DETAILS

Quantum mechanical calculations were performed using Gaussian 16 revision A.03.[41] The ωB97X-D density functional was selected as the main method of calculation because it can precisely describe non-covalent interactions, includes long-range exchange−correlation correction, and gives accurate chemical kinetics and thermodynamics results.[42−44] Also, the cost-effective triple-valence-zeta def2-TZVP[45,46] basis set was used to allow for relatively high accuracy while maintaining low computational cost.[47] The choice of the ωB97X-D/def2-TZVP level of theory was validated by comparing the optimized geometries of Me and Et with the available experimental and high-level structures. Figure S1 in the Supporting Information shows that the ωB97X-D/def2-TZVP level can reproduce experimental[48−51] and CASPT2 level[52,53] geometries at a high level of accuracy. Also, the experimentally determined dipole moments of Me (3.081 Debye[49]) and Et (3.39 Debye[54]) are available[50] and agree well with the values calculated at the ωB97X-D/def2-TZVP level (Me: 3.253 Debye and Et: 3.590 Debye). Therefore, ωB97X-D/def2-TZVP was considered adequate for the main quantum mechanical calculations.

In the second step, the conformers reported for Me[48] and Pr[55] were considered and all plausible conformers for Et, Pr, and Bu were generated. All conformers were optimized at the ωB97X-D/def2-TZVP level, and their Gibbs free energies (G) at 298.15 K and 1 atm were evaluated with respect to the most stable conformer (with the lowest G). The standard rigid rotor and harmonic oscillator approximations were used to compute G. Most input conformer structures converged into specific stable conformers. The outcome was 1, 2, 5, and 7 unique conformers for the Me, Et, Pr, and Bu ANs, respectively. To simplify further calculations, the most stable conformer was chosen, and all subsequent calculations were started from that structure. Later, conformational flexibility was introduced into the mechanism explorations to find all possible reaction products. All energies are reported relative to the most stable AN conformer.

The hydrolysis reactions were studied in water because the solvent is known to affect the kinetics of AN hydrolysis.[23,38] To simulate an aqueous solution, the reacting water molecule was considered explicitly and the reacting species were immersed in an implicit solvent medium modeled using the SMD[56] polarizable continuum model, which has been recently used in many studies.[57−61] This model can accurately describe ion−molecule interactions[62] without requiring solute cavity scaling.[63] The SMD-based implicit solvent treatment has been shown to outperform explicit water treatment in some studies.[64] Furthermore, application of this model is considered to be a highly accurate approach toward prediction of reaction free-energy barriers.[65,66]

In the next step, we performed systematic configurational sampling[67] to explore the diverse set of pre-reaction complexes that the reactants could form. The ABCluster 1.4 program,[68,69] which is based on the artificial bee colony (ABC) algorithm, was used to create 500 initial pre-reaction complexes for each reactant set. Then, 200 structures were generated from each initially created complex to search for the local and global minima geometries using 4 scout bees. At each generation round, the energy of the generated pre-reaction complexes were calculated as the summation of Columbic and Lennard-Jones interactions. For Columbic interactions, atomic polar tensor (APT) charges were calculated at the ωB97X-D/def2-TZVP level using the optimized reactants. For Lennard-Jones interactions, the parameters were taken from the study of Beckstein et al.[70] A total of 200 local minima (LM) geometries per reactant set were finally produced. Next, the LM structures were optimized at the GFN-xTB[71] semi-empirical level by the XTB 6.0.1[72] program. The optimized structures were then sorted based on their energy values and 50 of the structures with the lowest energies were re-optimized at the ωB97X-D/def2-TZVP level using Gaussian 16. After that, the structure with the lowest G value was chosen to represent the global minima (GM). Finally, the GM and some of the low-lying LM structures were selected for reaction coordinate scanning jobs to explore the plausible reaction paths.

To scan the reaction paths, several scenarios were considered. For the reaction of ANs with a single water molecule, water was treated mainly as a nucleophilic agent[36,37] that might cleave into OH and H upon reaction. Also, the inhibitory/catalytic role of water in auto-cleavage/intramolecular rearrangement of ANs was studied as a possible alternative. For the AN reaction with OH^-, nucleophilic substitution and hydrogen elimination were considered, as these two types of reactions have been proposed and confirmed in basic AN hydrolysis studies.[35,36,38,39] For acidic hydrolysis, more scenarios were investigated. First, the reaction of ANs with H_3O^+ was studied by focusing on the attack of H_3O^+ and the possibility of its intervention in intermolecular rearrangement/cleavage of ANs. In another scenario, the nucleophilic reaction of H_2O with protonated ANs was evaluated (see Figure 1 for geometries of the protonated ANs and the protonation G values, which will be addressed in the "Results and Discussion" section). Finally, unimolecular dissociation of the protonated ANs into HNO_3 and R^+ cations followed by nucleophilic addition of H_2O was studied, as this has been suggested as a plausible reaction scheme under acidic

https://dx.doi.org/10.1021/acsearthspacechem.0c00253
ACS Earth Space Chem. 2021, 5, 210−225

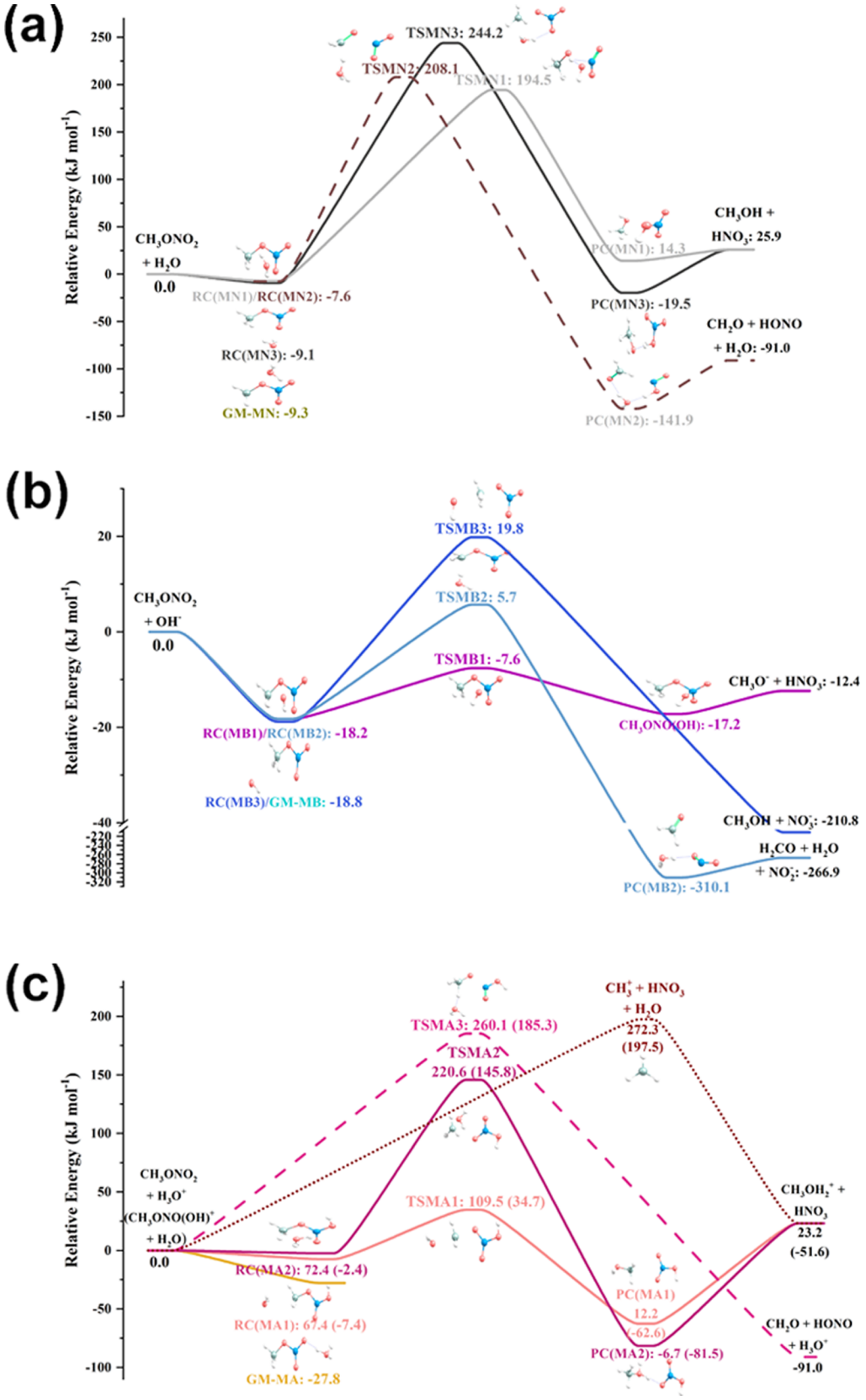

Figure 2. ZPE-corrected PES of the methyl nitrate (Me) reaction with H_2O (neutral hydrolysis), OH^- (basic hydrolysis), and H_3O^+ (acidic hydrolysis) (at 0 K). The reaction paths of neutral, basic, and acidic Me hydrolysis with barrier heights above 300, 150, and 200 kJ mol^{-1}, respectively, are shown in Figure S2. The red, blue, gray, and white spheres represent the oxygen, nitrogen, carbon, and hydrogen atoms, respectively.

https://dx.doi.org/10.1021/acsearthspacechem.0c00253
ACS Earth Space Chem. 2021, 5, 210−225

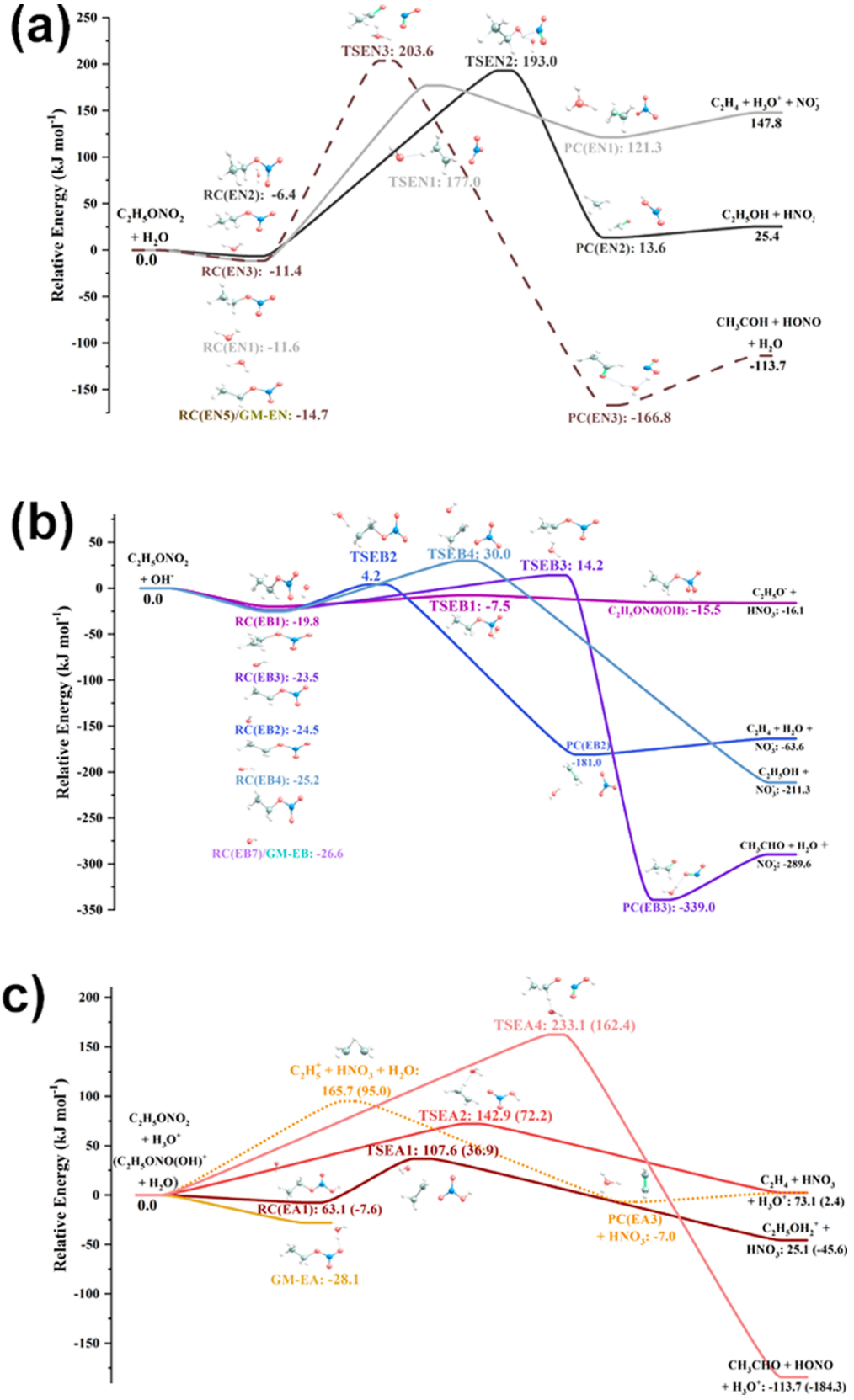

Figure 3. ZPE-corrected PES of the ethyl nitrate (Et) reaction with H_2O (neutral hydrolysis), OH^- (basic hydrolysis), and H_3O^+ (acidic hydrolysis) (at 0 K). The reaction paths of neutral, basic, and acidic Et hydrolysis with barrier heights above 300, 150, and 200 kJ mol^{-1}, respectively, are shown in Figure S3. The red, blue, gray, and white spheres represent the oxygen, nitrogen, carbon, and hydrogen atoms, respectively.

https://dx.doi.org/10.1021/acsearthspacechem.0c00253
ACS Earth Space Chem. 2021, 5, 210−225

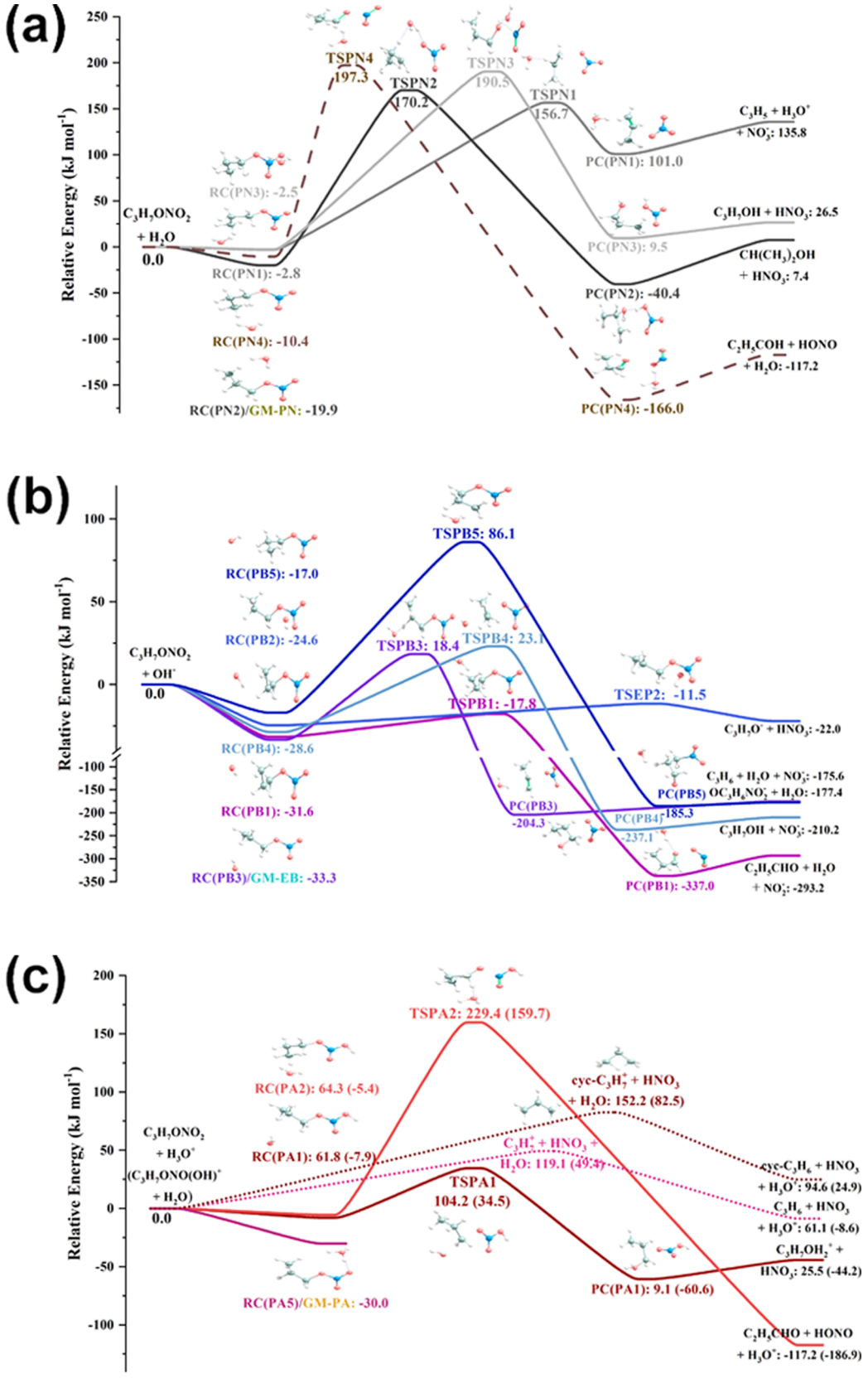

Figure 4. ZPE-corrected PES of the propyl nitrate (Pr) reaction with H_2O (neutral hydrolysis), OH^- (basic hydrolysis), and H_3O^+ (acidic hydrolysis) (at 0 K). The reaction paths of neutral, basic, and acidic Pr hydrolysis with barrier heights above 300, 150, and 200 kJ mol^{-1}, respectively, are shown in Figure S4. The red, blue, gray, and white spheres represent the oxygen, nitrogen, carbon, and hydrogen atoms, respectively.

https://dx.doi.org/10.1021/acsearthspacechem.0c00253
ACS Earth Space Chem. 2021, 5, 210−225

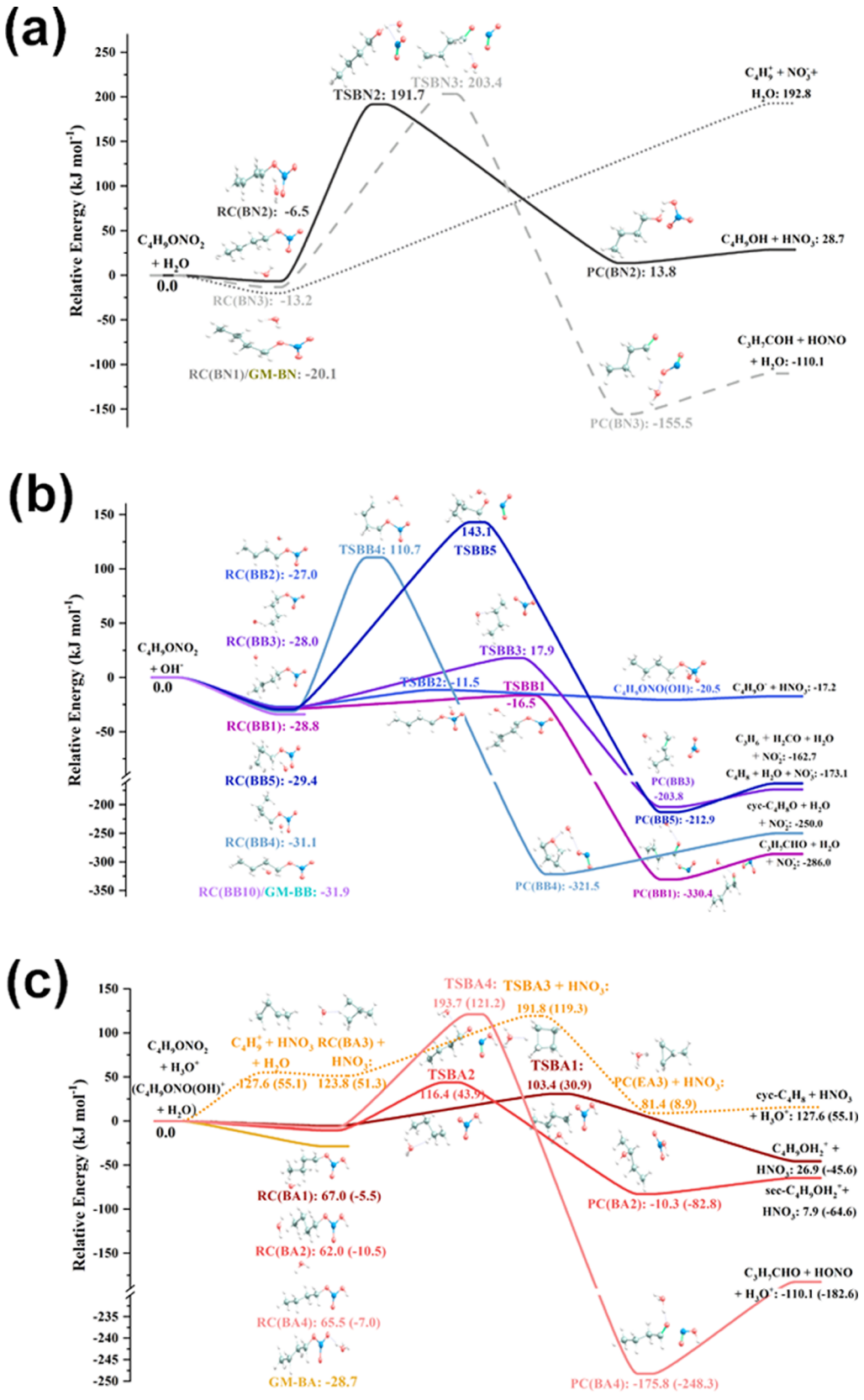

Figure 5. ZPE-corrected PES of the butyl nitrate (Bu) reaction with H_2O (neutral hydrolysis), OH^- (basic hydrolysis), and H_3O^+ (acidic hydrolysis) (at 0 K). The reaction paths of neutral, basic, and acidic Bu hydrolysis with barrier heights above 300, 150, and 200 kJ mol^{-1}, respectively, are shown in Figure S5. The red, blue, gray, and white spheres represent the oxygen, nitrogen, carbon, and hydrogen atoms, respectively.

https://dx.doi.org/10.1021/acsearthspacechem.0c00253
ACS Earth Space Chem. 2021, 5, 210−225

conditions by Rindelaub et al.[23] In either scenario, any identified TS was subjected to further investigation.

When the scanning approach failed to give plausible product formation paths, the configuration of the reacting species and the conformation of the ANs were manually changed to generate a guess transition state (TS) structure. Regardless of whether the TSs were identified using reaction coordinate scanning or by manual guesses, their harmonic frequencies were checked. After observation of a reasonable imaginary frequency for each TS candidate, intrinsic reaction coordinate (IRC)[73,74] analysis was performed to connect the TS to its corresponding pre- and post-reaction complexes. The pre- and post-reaction complexes were optimized and their nature was confirmed by the lack of imaginary frequencies. When the pre- and post-reaction complexes gave imaginary frequencies, the TS was assumed to yield the related reactants or products directly. Meanwhile, the reaction paths with no explicit TS, particularly the unimolecular dissociation paths, were confirmed using step-wise path scanning. In the end, the obtained reaction profiles were refined by performing single-point energy calculations at the CCSD(T)/cc-pVDZ level[75−77] (SMD solvent) on top of the geometries optimized at the ωB97X-D/def2-TZVP level to improve the accuracy of the energy values. Notably, in our initial assessment on two relatively identical reaction paths of methyl nitrate + water, CCSD(T)/cc-pVDZ was proved to give the lowest error in barrier height prediction relative to the CCSD(T)/aug-cc-pVTZ level (2.13% as compared to 3.92% for CCSD(T)/cc-pVTZ with the SMD model and 4.52% for DLPNO-CCSD(T)/aug-cc-pVTZ with the CPCMC solvent model performed using Orca 4.1.1[78]). The approximate CPU times for the TSs' single-point energy calculations at the CCSD(T)/cc-pVDZ, CCSD(T)/cc-pVTZ, DLPNO-CCSD(T)/aug-cc-pVTZ, and CCSD(T)/aug-cc-pVTZ levels were, respectively, 0.5, 22, 0.4, and 671.5 h.

RESULTS AND DISCUSSION

Reaction Mechanism. We investigated the reaction of four AN species, that is, methyl (Me), ethyl (Et), propyl (Pr), and butyl (Bu) nitrates with H_2O, OH^-, and H_3O^+, relevant to neutral, basic, and acidic conditions, respectively. In this way, a total of 12 potential energy surfaces (PESs) were obtained for the hydrolysis of the four ANs. Each PES contained a large number of different reaction pathways. To simplify the visualization of PESs, reaction paths with similar TSs, products, and energy profiles are illustrated by just one representative reaction path. Also, to enhance the visual efficiency of the PESs, the reaction paths are divided into two categories of high and low barrier height. The reaction paths with the lowest barrier heights are shown in the main PES figures (Figures 2−5), while the neutral, basic, and acidic reaction paths with zero-point energy (ZPE)-corrected barrier heights above 300, 150, and 200 kJ mol^{-1} (at 0 K), respectively, are reported in the Supporting Information (see Figures S2−S5). Also, the reaction paths with the lowest TS for the 12 reaction sets are displayed in Figure S6. Furthermore, to distinguish between the reaction species/paths, each TS and pre- (RC) and post-reaction (PC) complex is named after the corresponding AN and reaction condition. For instance, the species related to neutral, basic, and acidic hydrolysis of propyl nitrate [abbreviated as P (not Pr) in the naming of the PES species] were named using a combination of their nature (TS, RC, or PC) and PN (neutral Pr hydrolysis), PB (basic Pr hydrolysis), or PA (acidic Pr hydrolysis), respectively. In addition, the reaction paths of each PES were distinguished using a numerical identifier. Thus, the TS with the lowest barrier height, for example, for basic hydrolysis of butyl nitrate (BB) was called TSBB1, and the same numerical order was used for its connecting RC and PC complexes. In other words, all reaction paths were sorted and numbered according to their ascending barrier heights. We also note that for the acidic hydrolysis PESs, two general sets of reactants were considered; AN + H_3O^+ and protonated AN + H_2O (species' relative energies for the latter are reported relative to both AN + H_3O^+ (out of parenthesis) and protonated AN + H_2O (in parenthesis) throughout the figures and the text). Because of the large number of reactions and reaction paths, only the general and the most important features of the reaction mechanisms are discussed here (see the Supporting Information for the full computational data).

The most obvious feature of Figures 2−5 and S2−S5 is that all reaction paths can be considered single-step, in which only a single TS is involved. Another main feature is that the potential energy surfaces contain many RC complexes with different energies and configurations that connect to TSs with widely varying barrier heights and lead to a large variety of PC complexes. For some reaction paths, the RC and/or PC complexes are missing, for example, see the reaction path of TSEA2 in Figure 3, and we assume that in these cases, the TS connects directly to the separated reactants and/or products.

Another notable feature is that the most stable reactant complex does not necessarily connect to the lowest-energy TS or even to any TS at all. This is especially pronounced for the acidic reactions. In the case of neutral Me hydrolysis (the MN reaction), the energy of the lowest-energy RC complex (RC(MN3): −9.1 kJ mol^{-1}) connected to a TS is very close to that of the global minimum (GM) reactant complex GM-MN (−9.3 kJ mol^{-1}), but the actual structures of the two complexes are quite different (see Figure 2). For basic hydrolysis of Me, Et, Pr, and Bu, neutral hydrolysis of Et, Pr, and Bu, and also acidic hydrolysis of Pr, the lowest-energy RC complexes are the GMs. However, a large energy gap and configuration dissimilarity can be observed for acidic Me, Et, and Bu hydrolysis: GM-MA: −27.8 kJ mol^{-1} versus RC(MA2): −20.7 kJ mol^{-1} (see Figure 2); GM-EA: −28.1 kJ mol^{-1} versus RC(EA7): −8.4 kJ mol^{-1} (see Figures 3 and S3); and GM-BA: −28.7 kJ mol^{-1} versus RC(BA6): −11.2 kJ mol^{-1} (see Figures 5 and S5).

The third feature is the relation between the kinetics and thermodynamics of the AN hydrolysis channels. The lowest-energy reaction paths do not necessarily give the most thermodynamically stable product sets. For instance, in acidic Et hydrolysis, the lowest barrier (TSEA1: 107.6 (36.9) kJ mol^{-1}) leads to a relatively stable product set ($C_2H_5OH_2^+$ + HNO_3: 25.1 (−45.6) kJ mol^{-1}), but the most stable reaction product (CH_3CHO + HONO + H_3O^+: −113.7 (−184.3) kJ mol^{-1}) refers to TSEA4 (233.1 (162.4) kJ mol^{-1}) and TSEA7 (227.5 kJ mol^{-1}).

Two main factors affect kinetics of the reactions: ring strain in the TSs and higher nucleophilicity of the N site. For example, in the AN + H_2O → alcohol + HNO_3 reaction outlined in many studies,[23,36−38] the H_2O molecule can attack both carbon and nitrogen sites, but the barrier height related to the attack on the N site is lower than that of the alkyl carbons because the negative partial charge of the bridging oxygen in C−O−NO_2 is more than that of the dangling oxygen atoms.

https://dx.doi.org/10.1021/acsearthspacechem.0c00253
ACS Earth Space Chem. 2021, 5, 210−225

Therefore, it is easier for the bridging oxygen to form hydrogen bonds with the water molecule and permit the nucleophilic attack of water oxygen on the positively charged nitrogen atom. Moreover, this interaction mode causes less ring strain in the TS structure compared to nucleophilic attack on the alkyl carbon. Ring strain is a significant factor in AN hydrolysis because most TS structures of acidic and neutral hydrolysis involve 4-membered ring structures, which need high energies to overcome, and result in high reaction barriers. For basic hydrolysis of Me, Et, Pr, and Bu, the main reaction trends are hydrogen abstraction and nucleophilic substitution. Therefore, there is no ring strain to hinder most reaction paths of basic hydrolysis.

As an outcome of ring strain and nucleophilicity, the lowest barrier for neutral hydrolysis of methyl nitrate (TSMN1, see Figure 2) is 194.5 kJ mol^{-1} and corresponds to nucleophilic attack on the nitrate site. TSMN3 (244.2 kJ mol^{-1}) and TSMN4 (253.0 kJ mol^{-1}) target the alkyl site and are above 50 kJ mol^{-1} higher in energy. These three paths lead to the same product, that is, $CH_3OH + HNO_3$: 25.9 kJ mol^{-1}. It should be noted that TSMN2 cannot be considered as a hydrolysis TS. For neutral hydrolysis of ethyl nitrate, we can see that the lowest TS (TSEN1: 177.0 kJ mol^{-1}) is a hydrogen abstraction reaction path leading to highly unstable products because of producing ion pairs ($C_2H_4 + H_3O^+ + NO_3^-$: 147.8 kJ mol^{-1}) while TSEN2 (193.0 kJ mol^{-1}) with a higher barrier height gives a more stable product set ($C_2H_5OH + HNO_3$: 25.4 kJ mol^{-1}). The prompt recombination of ion pairs in the reaction path corresponding to TSEN2 is prevented by the fact that the formed product ions are on opposite sides of the C_2H_4 moiety. The endothermicity of the reaction path is thus likely real and not just a simulation artifact. TSEN4 and TSEN5 are both more than 400 kJ mol^{-1} above the reactants, and they, respectively, lead to $CH_4 + CH_2O + HNO_3$ (74.3 kJ mol^{-1}) and $CH_3OH + CH_3ONO_2$ (82.5 kJ mol^{-1}) (Figure S3). Similar to TSMN2, TSEN3 cannot be considered as a hydrolysis TS.

Similar to the EN reaction set, TSPN1 (156.7 kJ mol^{-1}) is a hydrogen abstraction reaction giving an alkyl product ($C_3H_5 + H_3O^+ + NO_3^-$: 135.8 kJ mol^{-1}) while the next TSs (TSPN2: 170.2 kJ mol^{-1} and TSPN3: 190.5 kJ mol^{-1}), respectively, lead to the $CH(CH_3)_2OH$ ($+HNO_3$: 7.4 kJ mol^{-1}) and C_3H_7OH ($+HNO_3$: 26.5 kJ mol^{-1}) alcohols. For neutral Bu hydrolysis (BN), the only "hydrolysis" TS below the 300 kJ mol^{-1} barrier threshold is TSBN2 (191.7 kJ mol^{-1}), which gives $C_4H_9OH + HNO_3$ (28.7 kJ mol^{-1}). For BN, another noteworthy reaction path is the barrierless but endothermal unimolecular dissociation of Bu into $C_4H_9^+ + NO_3^-$ (192.8 kJ mol^{-1}), in the presence of water. Although the other ANs can also undergo endothermic unimolecular dissociation, unimolecular dissociation with the help of water under neutral conditions was just identified for Bu because of the higher potential of the butyl chain for accepting positive charge relative to shorter alkyl groups.

In basic hydrolysis, most reaction products are stable relative to the reactants and there exist several very low reaction barriers. For the four ANs, the most kinetically affordable reaction paths are those leading to alkoxy anions and nitric acid. For the MB, EB, PB, and BB reaction sets, the OH^- anion can target the N-site in the reaction channels corresponding to TSMB1 (−7.6 kJ mol^{-1}), TSEB1 (−7.5 kJ mol^{-1}), TSPB2 (−11.5 kJ mol^{-1}), and TSBB2 (−11.5 kJ mol^{-1}) to give an associative product which can later dissociate into HNO_3 and CH_3O^- (−12.4 kJ mol^{-1}), $C_2H_5O^-$ (−16.1 kJ mol^{-1}), $C_3H_7O^-$ (−22.0 kJ mol^{-1}), and $C_4H_9O^-$ (−17.2 kJ mol^{-1}), respectively. In the case of TSPB2, the associative product produced an imaginary frequency, indicating that the molecule resulting from OH^- addition to the nitrate group of Pr is unstable and should dissociate immediately into nitric acid and $C_3H_7O^-$. It should be added that for the PB and BB reaction sets, the lowest reaction barriers are related to the elimination of hydrogen from the C_α atoms (the first carbon atoms connected to the nitrate site) in TSPB1 (−17.8 kJ mol^{-1}) and TSBB1 (−16.5 kJ mol^{-1}), respectively, giving the very stable $H_2O + NO_2^-$ products along with the C_2H_5CHO (−293.2 kJ mol^{-1}) and C_3H_7CHO (−286.0 kJ mol^{-1}) carbonyls. The basic hydrolysis reactions have many TSs that are lower in energy relative to their neutral and acidic counterparts and give much more stable products. However, they are not individually discussed here.

In acidic hydrolysis, there are two types of pathways. The pathways associated with the protonated AN + H_2O reaction are mainly the lowest-lying reaction paths. On the other hand, the high-barrier reaction paths related to the reaction of AN + H_3O^+ resemble the neutral hydrolysis pathways to some extent. For instance, the lowest TS associated with the reaction of methyl nitrate with H_3O^+ (TSMA4: 201.9 kJ mol^{-1}; note that TSMA1 to TSMA3 refer to the protonated methyl nitrate reaction with water) produces nitric acid and methanol ($CH_3OH_2^+ + HNO_3$: 23.2 kJ mol^{-1}; like neutral hydrolysis). However, the produced methanol molecule is protonated and the product set is a result of nucleophilic attack of H_3O^+ on the methyl group and donation of a hydrogen atom by H_3O^+ to the nitrate site. For the reactions of Et, Pr, and Bu with H_3O^+, the lowest-hydrolysis TSs are, respectively, TSEA6 (216.5 kJ mol^{-1}), TSPA5 (286.6 kJ mol^{-1}), and TSBA7 (293.1 kJ mol^{-1}) and give the $CH_4 + CH_2O + NO_2^+ + H_2O$ (114.8 kJ mol^{-1}), $CH_3OH_2^+ + C_2H_5ONO_2$ (64.6 kJ mol^{-1}), and $C_3H_7ONO_2 + CH_3OH_2^+$ (66.4 kJ mol^{-1}) products. Importantly, the NO_2^+ product observed for acidic hydrolysis of ethyl nitrate has been detected by spectroscopy and cryoscopy of AN hydrolysis in concentrated sulfuric acid solutions.[36]

The reaction of H_2O with protonated ANs was also considered even though the protonation of ANs by H_3O^+ is not thermodynamically spontaneous, and the G values of AN protonation by H_3O^+ are above 70 kJ mol^{-1} for Me, Et, Pr, and Bu (see Figure 1). It should be added that although the G values of AN protonation by free H^+ are all below −400 kJ mol^{-1}, free H^+ does not exist in aqueous solutions and H^+ is always found attached to H_2O molecules or other solution-phase species. Therefore, protonation of AN by free H^+ is not possible. Anyway, in the protonated AN + H_2O reaction scenario, there are indeed some reaction paths with relatively low barrier heights. TSMA1, TSEA1, TSPA1, and TSBA1, with reaction barriers that are 109.5 (34.7), 107.6 (36.9), 104.2 (34.5), and 103.4 (30.9) kJ mol^{-1} high relative to their corresponding AN + H_3O^+ (protonated AN + H_2O) energy level, all represent type 2 nucleophilic substitution reactions, in which the nucleophilic attack of H_2O on C_α of the alkyl chains produces the $CH_3OH_2^+$ (23.2 (−51.6) kJ mol^{-1}), $C_2H_5OH_2^+$ (25.1 (−45.6) kJ mol^{-1}), $C_3H_7OH_2^+$ (25.5 (−44.2) kJ mol^{-1}), and $C_4H_9OH_2^+$ (26.9 (−45.6) kJ mol^{-1}) protonated alcohols along with HNO_3. Similarly, TSBA2 (116.4 (43.9) kJ mol^{-1}) gives a protonated alcohol and nitric acid, but the nucleophilic substitution reaction is mixed with tautomerization (hydrogen transfer from C_β to C_α; see Figure 5) ending up with a

https://dx.doi.org/10.1021/acsearthspacechem.0c00253
ACS Earth Space Chem. 2021, 5, 210−225

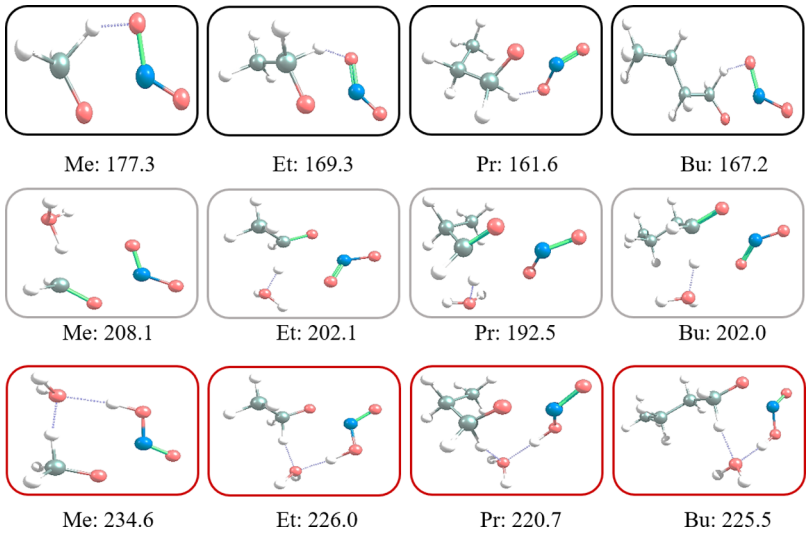

Figure 6. TS structures and barrier heights (in kJ mol^{-1}) of AN degradation into nitrous acid and carbonyl in the absence (black panels) and presence of water (gray panels) and hydronium ion (dark red panels) for methyl (Me), ethyl (Et), propyl (Pr), and butyl (Bu) nitrate.

secondary form of alcohol, that is, *sec*-$C_4H_9OH_2^+$: 17.9 (−54.6) kJ mol^{-1}. In contrast to neutral hydrolysis, these reactions involve nucleophilic attack on alkyl carbon and not the N-site. The reason is that here, one of the dangling nitrate oxygen atoms is protonated, which causes charge redistribution and makes the C−O−NO(OH) bond more susceptible for cleavage.

Another type of reaction path in acidic hydrolysis is unimolecular dissociation of the protonated ANs. As it can be seen in Figures 2−5, the dissociation products are less stable than the reactants, but the stability of the produced alkyl cations increases with chain length because longer chains can stabilize the positive charge better. Specifically, larger alkyls can undergo intramolecular changes to produce a more stable form of alkyl cation, which can easily donate its proton to a water molecule for larger protonated alkenes (Et, Pr, and Bu) or undergo water addition and protonated alcohol production in the case of CH_3^+. In any case, it should be recalled that both unimolecular dissociation and AN protonation by H_3O^+ are thermodynamically unfavorable. Therefore, these reaction paths should be treated cautiously in kinetics of acidic AN hydrolysis.

The fourth reaction scenario in acidic hydrolysis and also the second AN + H_2O reaction scenario refer to dissociation of the ANs into carbonyls and nitrous acid (HONO) in the presence of H_2O or H_3O^+; see TSMN2, TSMA6, TSEN3, TSEA7, TSPN4, TSPA4, TSBN3, and TSBA6. In the structure of these TSs, H_2O or H_3O^+ act as a bridge for transferring a H atom from C_α to the O atom of nitrate by abstracting the hydrogen atom from C_α and donating one of the H_2O/H_3O^+ hydrogen atoms to one of the dangling O atoms of the nitrate group. The question is: do H_2O and/or H_3O^+ catalyze the degradation reaction? According to Figure 6, the barrier heights related to intramolecular degradation of ANs into carbonyls and HONO in aqueous mediums are about 160−180 kJ mol^{-1}. However, when an adjacent water molecule intervenes in the H-transfer process and the break-down of the ANs, the barrier heights increase to 190−210 kJ mol^{-1}. The presence of H_3O^+ increases the barrier heights further (220−235 kJ mol^{-1}) and makes the degradation process less kinetically favorable. Therefore, H_2O and particularly H_3O^+ *inhibit* degradation of the ANs into carbonyls and HONO even though the PESs in Figures 2−5 and S2−S5 clearly show that these products are highly stable compared to the reactants. This finding might seem in conflict with the results of Rindelaub et al.[1] and Hu et al.,[27] who stated that acidity increases AN hydrolysis. However, we note that the degradation pathway studied here is just one possible AN elimination route, and the overall hydrolysis process may involve mechanisms missing from this study.

In addition to the discussed mechanistic details, the effect of alkyl chain length, the impact of acidity and basicity, and missing products should be addressed. In general, the diversity of products increases with alkyl chain length because more reaction paths are probable with increasing the number of C atoms. However, if we look at similar products, for example, alcohols + HNO_3, we can see that the relative energy of the associated TSs and products does not change significantly with chain length because the alkyl chains of the ANs do not change along the reaction paths. On the other hand, the products and energy profiles change significantly with the reaction conditions, that is, the reacting partner (OH^-, H_2O, or H_3O^+). Basic hydrolysis (i.e., the reaction of ANs with OH^-) provides many low barrier reaction paths that give thermodynamically stable reaction products, while most acidic hydrolysis routes involve either unstable products or high barriers resulted from low nucleophilicity of the attacked center and/or ring strain depending on the corresponding TS. The lowest barrier heights for the AN + H_3O^+ reactions are higher than those of neutral hydrolysis (TSMA4: 201.9 kJ mol^{-1} vs TSMN1: 194.5; TSEA6: 216.5 kJ mol^{-1} vs TSEN1: 177.0 kJ mol^{-1}; TSPA5: 286.6 kJ mol^{-1} vs TSPN1: 156.7 kJ mol^{-1}; and TSBA7: 293.1 kJ mol^{-1} vs TSBN1: 191.7 kJ mol^{-1}). Also, an important similarity between neutral and basic hydrolysis is that their most kinetically feasible reaction paths are associated with nucleophilic substitution toward alcohol/alkoxy ion + HNO_3/NO_3^-. This finding is in line with the study of Boschan et al.[36]

In the case of some reaction sets, many attempts were made to find reaction paths leading to the plausible products that could be guessed based on the structure of the ANs or similar reactions. Unfortunately, we were not able to find paths leading to some plausible product sets including CH_3OH + NO-

https://dx.doi.org/10.1021/acsearthspacechem.0c00253
ACS Earth Space Chem. 2021, 5, 210−225

Table 1. Total Diffusion-Modified ($k_{bi,i}^{mod}$) and the Total (Diffusion-Unmodified) ($k_{bi,i}$) Bimolecular Rate Coefficients (L mol^{-1} s^{-1}) of Methyl (Me), Ethyl (Et), Propyl (Pr), and Butyl (Bu) Nitrate Reaction under Neutral (Reaction with H_2O), Basic (Reaction with OH^-), and Acidic (Reaction with H_3O^+) Conditions

condition	Me	Et	Pr	Bu
		$k_{bi,i}^{mod}$		
neutral	6.93×10^{-27}	4.51×10^{-22}	6.82×10^{-18}	7.46×10^{-22}
basic	1.15×10^{9}	1.18×10^{9}	7.36×10^{9}	7.31×10^{9}
acidic	2.80×10^{-12}	3.22×10^{-11}	2.74×10^{-11}	5.30×10^{-11}
		$k_{bi,i}$		
neutral	6.93×10^{-27}	4.51×10^{-22}	6.82×10^{-18}	7.46×10^{-22}
basic	1.37×10^{9}	1.41×10^{9}	7.85×10^{11}	4.47×10^{11}
acidic	2.80×10^{-12}	3.22×10^{-11}	2.74×10^{-11}	5.30×10^{-11}

$(OH)_2^+$ and $CH_3OH + CH_3NO_2(OH)^+$ for acidic Et hydrolysis, $CH_4 + HOC_2H_4ONO_2$ and $C_2H_4 + H_2CO + H_3O^+$ for basic Pr hydrolysis, $CH_3O^- + C_2H_5ONO_2$ for neutral Et hydrolysis, $CH_3OH_2^+ + C_2H_4 + HNO_3$ for acidic Pr hydrolysis, $C_2H_5OH + C_2H_4 + HNO_3$ and $C_2H_5OH + C_2H_5ONO_2$ for neutral Bu hydrolysis, $C_2H_5OH + C_2H_4 + NO_3^-$ and $C_2H_5O^- + C_2H_5ONO_2$ for basic Bu hydrolysis, and $CH_3OH + C_3H_7ONO(OH)^+$ for acidic Bu hydrolysis. For the C_2H_4-containing product sets, the problem was that the tail hydrogen atom in the C_2H_5 moiety would move toward the C═C double bond to form a $\sigma-\pi$ bond. In some other cases, the guess TS structures were highly unstable and strained, breaking down into the proposed products immediately.

Reaction Rate Coefficients. The obtained PESs were transformed into rate coefficients (k), using transition state theory (TST) as this method has been adopted by many recent aqueous-phase studies, such as refs.[79−83] Among the available TST formulations, the tunneling-corrected bimolecular TST formulation (eq 1) was applied to all individual reaction paths.

$$k_{bi,r} = \kappa_r \times \frac{k_\beta T}{h}\left(\frac{RT}{p^\circ}\right) e^{-\Delta_r^\# G/RT} \quad (1)$$

In eq 1, $k_{bi,r}$ is the bimolecular rate coefficient for reaction path r, T is the temperature (298.15 K), h, k_B, and R parameters are, respectively, the Plank's, Boltzmann's, and universal gas constants, κ_r is the tunneling coefficient for reaction path r, p° is the reference pressure/concentration (=1 atm; RT/p° = 24.48 L mol^{-1}), and $\Delta_r^\# G$ is the Gibbs free energy of reaction along path r at 298.15 K and 1 atm. The reaction paths were described as one-dimensional unsymmetrical Eckart barriers[84] according to the formulation suggested by Shavitt[85] to obtain the κ_r values. $\Delta_r^\# G$ was calculated as the difference between the G value of the TSs (G_{TS}) and the G value of their corresponding reactants ($G_{reactants}$) (eq 2). The individual G values were computed by adding the thermal corrections (entropy and enthalpy contributions) from the ωB97X-D/def2-TZVP level ($G_{thermal}^{DFT}$) to the electronic energy values at the CCSD(T)/cc-pVDZ//ωB97X-D/def2-TZVP level (E_{CCSD}) (eq 3). For the protonated AN + H_2O reaction paths, $\Delta_r^\# G$ of the reaction was summed up with the associated protonation Gibbs free energies (reported in Figure 1) to account for the energy cost of AN protonation by H_3O^+.

$$\Delta_r^\# G = G_{TS} - G_{reactants} \quad (2)$$

$$G_{TSorreactants} = E_{CCSD} + G_{thermal}^{DFT} \quad (3)$$

By application of eq 2, the effects of the RC and PC complexes were ignored by assuming equilibrium between the reactants and RC complexes and feasible interconversion of the RC complexes into each other. When using this assumption, the exact energies of the RC complexes would not affect the $k_{bi,r}$ results.[86] Moreover, consideration of the interconversion of the RC and PC complexes and the use of steady-state approximation would neutralize the impact of the RC and PC complexes on the final rate coefficients.[87] Also, in the kinetic analysis, we treated all reaction paths as irreversible reactions, that is, reverse reactions were neglected. This assumption is likely valid at least for the paths leading to more than two products[88] or the paths with a highly volatile product that prefers diffusing to the gas phase.

In the next step, the total bimolecular rate coefficient related to the reaction of each AN with any of the OH^-, H_3O^+, or H_2O species ($k_{bi,i}$) was obtained by summing the $k_{bi,r}$ values related to that specific reaction set (see eq 4). Tables S1−S4 report the imaginary frequencies used for calculation of the tunneling coefficients, the applied $\Delta_r^\# G$ values, and the final $k_{bi,r}$ results for the four ANs.

$$k_{bi,i} = \sum_r k_{bi,r} \quad (4)$$

The obtained rate coefficients were corrected for the effects of solvent's degrees of freedom and restriction of the reaction by solvent dynamics (i.e., diffusion).[82] The impact of the solvent's degrees of freedom can appear as changes in the energy profiles. Therefore, the $\Delta_r^\# G$ values were extracted from quantum mechanical calculations in implicit water solvent using the SMD model. This treatment neglected the effect of other aqueous aerosol components on the energy profiles but captured the main feature of aqueous aerosol systems, that is, the presence of the water solvent. The influence of diffusion can limit the rate of fast chemical reactions by slowing down the diffusion of the reactants toward each other. To consider the diffusion effect, the rate coefficient of diffusion (k_{diff}) was calculated based on the Stokes−Einstein law[89,90] formulated in the simple form of eq 5.[91] In this equation, η is dynamic viscosity of the solution (pure water here) adopted from International Steam Tables.[92] After calculating k_{diff} (= 7.43 × 10^9 L mol^{-1} s^{-1} at 298.15 K), the $k_{bi,i}$ results (of the fast basic hydrolysis reactions) were modified for diffusion effects through eq 6 and the total diffusion-modified bimolecular rate coefficients of each reaction set i ($k_{bi,i}^{mod}$) were obtained. An important point is that cage effect on the rate coefficients[93] was excluded because the main focus of this study is hydrolysis and the cages are made of the H_2O reactant.

https://dx.doi.org/10.1021/acsearthspacechem.0c00253
ACS Earth Space Chem. 2021, 5, 210−225

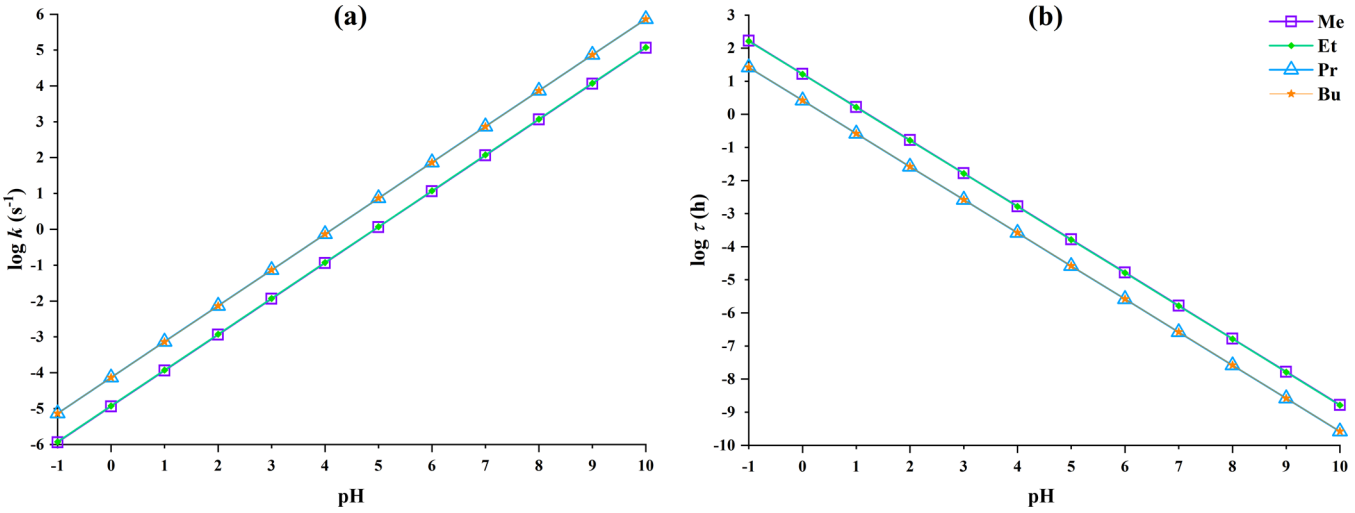

Figure 7. pH dependency of the pseudo-first-order total rate coefficients of methyl (Me), ethyl (Et), propyl (Pr), and butyl (Bu) nitrate hydrolysis at 298.15 K and 1 atm (a), along with the corresponding half-lives (Bu). See Table S5 for the corresponding values.

$$k_{\text{diff}} = \frac{8k_\beta T}{3\eta} \tag{5}$$

$$k_{\text{bi},i}^{\text{mod}} = \frac{k_{\text{bi},i} \times k_{\text{diff}}}{k_{\text{bi},i} + k_{\text{diff}}} \tag{6}$$

Using eq 6, the $k_{\text{bi},i}^{\text{mod}}$ values were calculated for the MN, MB, MA, EM, EB, EA, PM, PB, PA, BN, BB, and BA reaction sets and are reported in Table 1. These values directly reflect the energy profiles of Figures 2−5 (and S2−S5). The low barrier heights observed for the AN reaction with OH^- have caused large $k_{\text{bi,MB}}^{\text{mod}}$, $k_{\text{bi,EB}}^{\text{mod}}$, $k_{\text{bi,PB}}^{\text{mod}}$, and $k_{\text{bi,BB}}^{\text{mod}}$ values, and the high neutral reaction barriers have resulted in $k_{\text{bi},i}^{\text{mod}}$ values lower than 10^{-17} L mol^{-1} s^{-1}. In addition, the $k_{\text{bi},i}^{\text{mod}}$ results indicate that the kinetics of Et hydrolysis is similar to that of Me and the kinetics of Bu and Pr hydrolysis is similar.

To study the effect of pH and enable comparison of the hydrolysis process with first-order AN removal methods, the $k_{\text{bi},i}^{\text{mod}}$ values were converted into pseudo-first-order rate coefficients by multiplying by the concentration/activity of the OH^-, H_3O^+, and H_2O reactants, computed at each pH. The equilibrium concentrations of the OH^-, H_3O^+, and H_2O species (C_i) were considered equal to their activities to simplify the calculations. For H_2O concentration in aqueous aerosols (C_{H_2O}), the concentration range of 46.1−55.5 mol L^{-1} has been reported.[94] After applying the 46.1 and 55.5 mol L^{-1} values and observing insignificant changes in the final results, the average value of 50.8 mol L^{-1} was used for C_{H_2O}. For $C_{H_3O^+}$ and C_{OH^-}, eqs 7 and 8 were used, respectively. The pH was varied from −1 (highly acidic aerosols) to 10 (highly basic atmospheric aerosols)[95] and the pH-specific pseudo-first-order rate coefficients ($k_{\text{uni}}^{\text{tot}}$) were obtained using eq 9. In the end, the half-life (τ) of the ANs at each pH was calculated according to the pseudo-first-order results (eq 10).

$$C_{H_3O^+} = 10^{-\text{pH}}\ \text{mol/L} \tag{7}$$

$$C_{OH^-} = 10^{\text{pH}-14}\ \text{mol/L} \tag{8}$$

$$k_{\text{uni}}^{\text{tot}} = \sum_i k_{\text{bi},i}^{mod} \times C_i \tag{9}$$

$$\tau = \ln(2)/k_{\text{uni}}^{\text{tot}} \tag{10}$$

Figure 7 displays the pH-specific pseudo-first-order rate coefficients of Me, Et, Pr, and Bu hydrolysis, in addition to the obtained half-lives, and Table S5 summarizes the kinetics results in a numerical format. As it is evident in Figure 7a, the obtained pseudo-first-order rate coefficients of AN hydrolysis are quite pH-sensitive, as perceived in all experimental studies. However, in conflict with some earlier studies on acid-catalyzed hydrolysis, our predicted rate coefficients all increase sharply from about 10^{-6} s^{-1} to 10^5 s^{-1} with increasing pH from −1 to 10. The general belief in recent papers on AN hydrolysis is that highly acidic conditions enhance the rate of AN hydrolysis.[23,25,27,29,36] However, Figure 7 implies that acidity suppresses AN hydrolysis through limitation of basic hydrolysis even though the $k_{\text{bi},i}^{\text{mod}}$ values of Me, Et, Pr, and Bu acidic reaction sets are, respectively, 15, 11, 7, and 11 orders of magnitude higher than their neutral values. In fact, Figure 7 implies that OH^- availability is the main determinant of the hydrolysis extent. This is why we observe similar pH-dependency trends for the four ANs, and, based on the results, we expect the products of the AN reaction with OH^- (mainly alcohols, alkoxy ions, nitric acid, and NO_3^-) to be the major AN hydrolysis products over the whole evaluated pH range. Our results also imply that increased basicity prompts conversion of the ANs into the basic hydrolysis products, in agreement with the finding of Lucas and Hammett.[28]

Figure 7a also displays a sudden shift in the $k_{\text{uni}}^{\text{tot}}$ values causing similar kinetics for the Et and Me ANs on the one hand and for Pr and Bu on the other hand. This follows directly from the characteristics of the PESs shown in Figures 2−5 and S2−S5. The MB and EB reaction sets include just one path with zero apparent activation energy (at 0 K), while the PB and BB reaction sets contain 2 such paths. Although these paths are noticeably faster than the other reaction paths, there are several paths that have reaction barriers low enough to contribute to basic AN hydrolysis. The difference in the activation energies of these paths causes a slight change in the $k_{\text{bi},i}^{\text{mod}}$ and $k_{\text{uni}}^{\text{tot}}$ values from Et to Me and from Pr to Bu.

Furthermore, Figure 7b indicates that the increase in acidity prolongs AN lifetime in aqueous aerosols while the increase in basicity prompts AN removal through hydrolysis reactions.

https://dx.doi.org/10.1021/acsearthspacechem.0c00253
ACS Earth Space Chem. 2021, 5, 210−225

The effect of pH on half-life of the ANs is so intense that τ decreases from 1.67×10^2 h (for Me) to 2.64×10^{-10} h (for Bu) by increasing the pH from −1 to 10. At neutral pH, the τ values of Me, Et, Pr, and Bu, respectively, equal to 1.67×10^{-6}, 1.63×10^{-6}, 2.62×10^{-7}, and 2.63×10^{-7} h. These values imply that the studied ANs should be hydrolyzed in less than a millisecond and, therefore, they should not be measurable in neutral water. This is clearly invalid as methyl nitrate is detectable in neutral water.[96] Therefore, the calculated half-lives are not reliable based on experimental evidences, although they directly follow the PESs. Many of the lowest-barrier basic hydrolysis pathways have reaction free energies close to zero and could thus be thermodynamically rather than kinetically limited (In other words, our assumption of irreversible reactions may be wrong especially for these pathways). However, for each AN, there exists at least one basic hydrolysis pathway with a barrier lower than 10 kJ mol^{-1} and a reaction free energy lower than −100 kJ mol^{-1}. Thermodynamic limitations on basic hydrolysis can thus not explain most of the discrepancy between our results and experiments.

To further evaluate the validity of the kinetics results, the calculated half-lives and k_{uni}^{tot} values were compared with the experimental data available for the studied ANs and any similar AN. The only kinetics data that fully accomplishes the considered pH and temperature conditions is the half-life of Et hydrolysis in 55 wt % D_2SO_4 solution at 296 ± 2 K, which is reported as 2.5 h ($k_{uni}^{tot} \approx 9.97 \times 10^2$ s^{-1}) by Hu et al.[27] Roughly estimating, a 55 wt % D_2SO_4 solution should have a pH around −1. At pH −1, the half-life of Et is calculated as 163 h and, at pH 0, τ_{Et} is 16.3 h. Hu et al.[27] mentioned that their results might be biased by HNO_3 hydrolysis giving a trend of AN hydrolysis kinetics faster than what can be expected. They also argued that the reactions driven by the aqueous-phase NO_x ions should have enhanced the loss of ethyl nitrate beyond the expected hydrolysis trend. On the other hand, our theoretical results are based on many assumptions and the obtained energy profiles and barrier heights might be inaccurate by several to tens of kJ mol^{-1}. Therefore, the true half-life of Et hydrolysis could be something in between the experimentally and theoretically observed values.

McKinley-McKee and Moelwyn-Hughes[96] reported the empirical relationship of $\log k\ (s^{-1}) = 75.3243 - 21.4319 \log T - 9229.03/T$ for Me hydrolysis in pure water (pH 7) over the temperature range of 343−414 K. They noted that the reaction is first order under their studied conditions. Supposing the relationship can be extended to the temperature of 298.15 K, this relationship gives the rate coefficient of 2.18×10^{-9} s^{-1} ($\tau_{Me} = 8.84 \times 10^4$ h), while we calculated the k_{uni}^{tot} value of 1.15×10^2 s^{-1} ($\tau_{Me} = 1.67 \times 10^{-6}$ h) for pH 7. In addition, McKinley-McKee and Moelwyn-Hughes observed non-negligible temperature dependency. In other words, their results suggested that there is a significant reaction barrier for the overall hydrolysis reaction. However, our kinetics results showed that the overall process is dominated by basic hydrolysis, which is mainly controlled by low-barrier reaction paths.

Moreover, as mentioned, the kinetics of Me and Et hydrolysis is almost identical, and their pH-dependency trend are similar to that of Pr and Bu. Therefore, the results of Hu et al.[27] ($k_{uni}^{tot} \approx 9.97 \times 10^2$ s^{-1} at pH −1 for Et hydrolysis) and McKinley-McKee and Moelwyn-Hughes[96] ($k_{uni}^{tot} = 2.18 \times 10^{-9}$ s^{-1} at pH 7) can be used to compare the experimental and theoretical trends of pH dependency. Although the outlined experimental values suggest a sharp negative pH dependency for hydrolysis of the ANs over the pH range of −1−7, our theoretical results indicate sharp positive pH dependency. All these discrepancies point out that there probably exists an acidic hydrolysis mechanism missing from our study.

Finally, the kinetics of Pr and Bu hydrolysis (as straight-chain ANs) should be compared with the kinetics of isopropyl (IPr) and (IBu) isobutyl nitrates (as-branched ANs). Rindelaub et al.[23] observed that the rate coefficients of IP and IB hydrolysis are quite similar over the pH range of 0.25−4 and close to each other at pH 7. This finding is in line with our results suggesting that similar kinetics should be observed for similar ANs. Also, they reported that the average rate coefficient for IPr and IBu hydrolysis decreases from 1.1×10^{-5} to 1.23×10^{-7} s^{-1} by increasing pH from 0.25 to 6.9. Therefore, they observed smooth negative pH dependency for IPr and IBu, contrarily to our theoretically predicted sharp positive pH dependency for Pr and Bu.

In general, the observed conflicts suggest several scenarios to be evaluated in future studies: (1) cross-reactions between OH^- and the products of AN hydrolysis as such reactions can limit the OH^- concentration available to basic hydrolysis; (2) reversibility of the low-barrier basic hydrolysis paths; and (3) the catalytic effect of additional (explicit) water molecules for both neutral and acidic hydrolysis. These scenarios might lead to a decrease in the basic hydrolysis rate by limiting low-barrier basic hydrolysis paths, while introducing some new kinetically feasible acidic pathways.

CONCLUSIONS

As an important process participating in the nitrogen cycle and a permanent sink for NOx, kinetics of alkyl nitrate (AN) hydrolysis in aqueous aerosols was studied using quantum mechanical and chemical kinetics methods for methyl, ethyl, propyl, and butyl nitrates. The overall hydrolysis process was described as a combination of basic, neutral, and acidic hydrolysis. According to our results, basic hydrolysis is kinetically fast, and it gives thermodynamically stable products including alkenes, alcohols, alkoxy ions, highly water-soluble NOx ions (such as NO_3^-), and HNO_3. The extent of the neutral hydrolysis reaction is limited by high energy barriers and all neutral hydrolysis products (the alkenes, alkanes, and NOx ions as minor products and alcohols and HNO_3 as major products) are relatively unstable. Acidic hydrolysis follows a more complicated scheme, in which the hydronium ion can react with the ANs or the ANs can be first protonated and then react with water. Although the reaction of protonated ANs with water is kinetically more favorable than neutral hydrolysis and AN reaction with the hydronium ion, both types of acidic pathways result in slow hydrolysis kinetics. In either case, acidic hydrolysis mainly gives protonated alcohols and HNO_3. Both neutral and acidic processes were found to be incapable of promoting intramolecular degradation of the ANs. Furthermore, calculation of the pH-specific first-order rate coefficients and comparison with the available experimental data indicated that an acidic hydrolysis mechanism is likely missing from our proposed reaction mechanism. The missing mechanism would be responsible for the "acidic catalysis" addressed in many experimental studies. In addition, the reaction barriers and/or energies of our basic hydrolysis mechanisms may be too low, as the experimentally measured temperature dependence of hydrolysis rates indicates the

https://dx.doi.org/10.1021/acsearthspacechem.0c00253
ACS Earth Space Chem. 2021, 5, 210−225

existence of non-negligible energy barriers. Therefore, the reliability of our results for mechanistic description of AN hydrolysis varies with the pH of the aerosol in question. In acidic to neutral rain (pH: 3.5−6.5), marine/polluted cloud (pH: 3.6−6), remote cloud (pH: 4−6), continental cloud (pH: 3.9−5.0), polluted cloud (pH: 2−5), polluted fog (pH: 2−7), continental fog (pH: 3.8−7.2), remote fog (pH: 3.1−7.4), sea fog (pH: 4.8−6.1), marine aerosols (pH: −1−10), urban aerosol (pH: −2−5), continental aerosols (pH: −0.8−4.5), and haze (pH: −2.5−8),[95] there might be some unexplored reaction mechanisms or cross-reactions responsible for improved hydrolysis of ANs. In basic marine and haze aerosols, our calculations might be to some extent biased by the inevitably present error sources in the chosen level of theory. Also, the chemistry of aqueous aerosols (i.e., the presence of other species) can alter the reported energy profiles and reduce or increase the extent of AN hydrolysis.

■ ASSOCIATED CONTENT

Supporting Information

The Supporting Information is available free of charge at https://pubs.acs.org/doi/10.1021/acsearthspacechem.0c00253.

Comparison of the optimized geometries with experimental structures, hydrolysis paths with high reaction barriers, the lowest-barrier hydrolysis paths of all reactions, the data used to calculate the rate coefficients, and the numerical values of all pH-specific half-lives and pseudo-first-order rate coefficients (PDF)

Output files of frequency and CCSD(T)/cc-pVDZ single-point energy calculations (ZIP)

■ AUTHOR INFORMATION

Corresponding Author

Fatemeh Keshavarz − *Institute for Atmospheric and Earth System Research, Faculty of Science, University of Helsinki, Helsinki FI-00014, Finland;* orcid.org/0000-0003-2189-7809; Email: fatemeh.keshavarz@helsinki.fi

Authors

Joel A. Thornton − *Department of Atmospheric Science, University of Washington, Seattle, Washington 98195, United States*

Hanna Vehkamäki − *Institute for Atmospheric and Earth System Research, Faculty of Science, University of Helsinki, Helsinki FI-00014, Finland;* orcid.org/0000-0002-5018-1255

Theo Kurtén − *Department of Chemistry, Faculty of Science, University of Helsinki, Helsinki FI-00014, Finland;* orcid.org/0000-0002-6416-4931

Complete contact information is available at: https://pubs.acs.org/10.1021/acsearthspacechem.0c00253

Notes

The authors declare no competing financial interest.

■ ACKNOWLEDGMENTS

Financial support by Academy of Finland and the ERC Project 692891-DAMOCLES and computational resources provided by the CSC-IT Center for Science in Espoo, Finland, are highly appreciated.

■ REFERENCES

(1) Rindelaub, J. D.; McAvey, K. M.; Shepson, P. B. Determination of α-pinene-derived organic nitrate yields: particle phase partitioning and hydrolysis. *Atmos. Chem. Phys. Discuss.* **2014**, *14*, 3301−3335.

(2) Finlayson-Pitts, B. J.; Pitts, J. N. Tropospheric air pollution: ozone, airborne toxics, polycyclic aromatic hydrocarbons, and particles. *Science* **1997**, *276*, 1045−1051.

(3) Browne, E. C.; Cohen, R. C. Effects of biogenic nitrate chemistry on the NO x lifetime in remote continental regions. *Atmos. Chem. Phys.* **2012**, *12*, 11917−11932.

(4) He, S.; Chen, Z.; Zhang, X. Photochemical reactions of methyl and ethyl nitrate: a dual role for alkyl nitrates in the nitrogen cycle. *Environ. Chem.* **2011**, *8*, 529−542.

(5) Ammann, M.; Cox, R. A.; Crowley, J. N.; Jenkin, M. E.; Mellouki, A.; Rossi, M. A.; Troe, J.; Wallington, T. J. IUPAC Task Group on Atmospheric Chemical Kinetic Data Evaluation, 2016. http://iupac.pole-ether.fr/index.html (last accessed May 2020).

(6) Flocke, F.; Volz-Thomas, A.; Buers, H.-J.; Pätz, W.; Garthe, H.-J.; Kley, D. Long-term measurements of alkyl nitrates in southern Germany: 1. General behavior and seasonal and diurnal variation. *J. Geophys. Res. Atmos.* **1998**, *103*, 5729−5746.

(7) Sander, S. P.; Golden, D. M.; Kurylo, M. J.; Moortgat, G. K.; Wine, P. H.; Ravishankara, A. R.; Kolb, C. E.; Molina, M. J.; Finlayson-Pitts, B. J.; Huie, R. E.; et al. *Chemical Kinetics and Photochemical Data for Use in Atmospheric Studies Evaluation Number 15*; Jet Propulsion Laboratory, National Aeronautics and Space Administration: Pasadena, CA, 2006.

(8) Liebmann, J.; Sobanski, N.; Schuladen, J.; Karu, E.; Hellén, H.; Hakola, H.; Zha, Q.; Ehn, M.; Riva, M.; Heikkinen, L.; et al. Alkyl nitrates in the boreal forest: formation via the NO3-, OH- and O3-induced oxidation of biogenic volatile organic compounds and ambient lifetimes. *Atmos. Chem. Phys.* **2019**, *19*, 10391−10403.

(9) Sobanski, N.; Thieser, J.; Schuladen, J.; Sauvage, C.; Song, W.; Williams, J.; Lelieveld, J.; Crowley, J. N. Day and night-time formation of organic nitrates at a forested mountain site in south-west Germany. *Atmos. Chem. Phys.* **2017**, *17*, 4115−4130.

(10) Ng, N. L.; Brown, S. S.; Archibald, A. T.; Atlas, E.; Cohen, R. C.; Crowley, J. N.; Day, D. A.; Donahue, N. M.; Fry, J. L.; Fuchs, H.; et al. Nitrate radicals and biogenic volatile organic compounds: oxidation, mechanisms, and organic aerosol. *Atmos. Chem. Phys.* **2017**, *17*, 2103−2162.

(11) Wayne, R. P.; Barnes, I.; Biggs, P.; Burrows, J. P.; Canosa-Mas, C. E.; Hjorth, J.; Le Bras, G.; Moortgat, G. K.; Perner, D.; Poulet, G.; et al. The nitrate radical: physics, chemistry, and the atmosphere. *Atmos. Environ., Part A* **1991**, *25*, 1−203.

(12) Luke, W. T.; Dickerson, R. R.; Nunnermacker, L. J. Direct measurements of the photolysis rate coefficients and Henry's law constants of several alkyl nitrates. *J. Geophys. Res. Atmos.* **1989**, *94*, 14905−14921.

(13) Ng, M.; Mok, D. K. W.; Lee, E. P. F.; Dyke, J. M. The atmospherically important reaction of hydroxyl radicals with methyl nitrate: a theoretical study involving the calculation of reaction mechanisms, enthalpies, activation energies, and rate coefficients. *J. Phys. Chem. A* **2017**, *121*, 6554−6567.

(14) Ballschmiter, K. ATMOSPHERIC CHEMISTRY: A Marine Source for Alkyl Nitrates. *Science* **2002**, *297*, 1127−1128.

(15) Chuck, A. L.; Turner, S. M.; Liss, P. S. Direct evidence for a marine source of C1 and C2 alkyl nitrates. *Science* **2002**, *297*, 1151−1154.

(16) Darnall, K. R.; Carter, W. P. L.; Winer, A. M.; Lloyd, A. C.; Pitts, J. N., Jr Importance of RO2 + nitric oxide in alkyl nitrate formation from C4-C6 alkane photooxidations under simulated atmospheric conditions. *J. Phys. Chem.* **1976**, *80*, 1948−1950.

(17) Simpson, I. J.; Meinardi, S.; Blake, D. R.; Blake, N. J.; Sherwood Rowland, F.; Atlas, E.; Flocke, F. A biomass burning source of C1−C4 alkyl nitrates. *Geophys. Res. Lett.* **2002**, *29*, 2168−2171.

(18) Lockwood, A. L.; Filley, T. R.; Rhodes, D.; Shepson, P. B. Foliar uptake of atmospheric organic nitrates. *Geophys. Res. Lett.* **2008**, *35*, L15809.

(19) Paulot, F.; Henze, D. K.; Wennberg, P. O. Impact of the isoprene photochemical cascade on tropical ozone. *Atmos. Chem. Phys.* **2012**, *12*, 1307−1325.
(20) Zare, A.; Romer, P. S.; Nguyen, T.; Keutsch, F. N.; Skog, K.; Cohen, R. C. A comprehensive organic nitrate chemistry: insights into the lifetime of atmospheric organic nitrates. *Atmos. Chem. Phys.* **2018**, *18*, 15419−15436.
(21) Roberts, J. M. The atmospheric chemistry of organic nitrates. *Atmos. Environ., Part A* **1990**, *24*, 243−287.
(22) Perraud, V.; Bruns, E. A.; Ezell, M. J.; Johnson, S. N.; Yu, Y.; Alexander, M. L.; Zelenyuk, A.; Imre, D.; Chang, W. L.; Dabdub, D.; et al. Nonequilibrium atmospheric secondary organic aerosol formation and growth. *Proc. Natl. Acad. Sci.* **2012**, *109*, 2836−2841.
(23) Rindelaub, J. D.; Borca, C. H.; Hostetler, M. A.; Slade, J. H.; Lipton, M. A.; Slipchenko, L. V.; Shepson, P. B. The acid-catalyzed hydrolysis of an α-pinene-derived organic nitrate: kinetics, products, reaction mechanisms, and atmospheric impact. *Atmos. Chem. Phys.* **2016**, *16*, 15425−15432.
(24) Fisher, J. A.; Jacob, D. J.; Travis, K. R.; Kim, P. S.; Marais, E. A.; Chan Miller, C.; Yu, K.; Zhu, L.; Yantosca, R. M.; Sulprizio, M. P.; et al. Organic nitrate chemistry and its implications for nitrogen budgets in an isoprene- and monoterpene-rich atmosphere: constraints from aircraft (SEAC4RS) and ground-based (SOAS) observations in the Southeast US. *Atmos. Chem. Phys.* **2016**, *16*, 5969−5991.
(25) Zare, A.; Fahey, K. M.; Sarwar, G.; Cohen, R. C.; Pye, H. O. T. Vapor-pressure pathways initiate but hydrolysis products dominate the aerosol estimated from organic nitrates. *ACS Earth Space Chem.* **2019**, *3*, 1426−1437.
(26) Carlton, A. G.; Turpin, B. J. Particle partitioning potential of organic compounds is highest in the Eastern US and driven by anthropogenic water. *Atmos. Chem. Phys.* **2013**, *13*, 10203−10214.
(27) Hu, K. S.; Darer, A. I.; Elrod, M. J. Thermodynamics and kinetics of the hydrolysis of atmospherically relevant organonitrates and organosulfates. *Atmos. Chem. Phys.* **2011**, *11*, 8307−8320.
(28) Lucas, G. R.; Hammett, L. P. Rate and Mechanism in the Reactions of t-Butyl Nitrate and of Benzyl Nitrate with Water and with Hydroxyl Ion1. *J. Am. Chem. Soc.* **1942**, *64*, 1928−1937.
(29) Rindelaub, J. D.; McAvey, K. M.; Shepson, P. B. The photochemical production of organic nitrates from α-pinene and loss via acid-dependent particle phase hydrolysis. *Atmos. Environ.* **2015**, *100*, 193−201.
(30) Bean, J. K.; Hildebrandt Ruiz, L. Gas−particle partitioning and hydrolysis of organic nitrates formed from the oxidation of α-pinene in environmental chamber experiments. *Atmos. Chem. Phys.* **2016**, *16*, 2175−2184.
(31) Chuang, W. K.; Donahue, N. M. A two-dimensional volatility basis set − Part 3: Prognostic modeling and NOx dependence. *Atmos. Chem. Phys. Discuss.* **2016**, *16*, 123−134.
(32) Liu, S.; Shilling, J. E.; Song, C.; Hiranuma, N.; Zaveri, R. A.; Russell, L. M. Hydrolysis of organonitrate functional groups in aerosol particles. *Aerosol Sci. Technol.* **2012**, *46*, 1359−1369.
(33) Boyd, C. M.; Sanchez, J.; Xu, L.; Eugene, A. J.; Nah, T.; Tuet, W. Y.; Guzman, M. I.; Ng, N. L. Secondary organic aerosol formation from the β-pinene+NO3 system: effect of humidity and peroxy radical fate. *Atmos. Chem. Phys.* **2015**, *15*, 7497−7522.
(34) Hoffsommer, J. C.; Glover, D. J.; Burlinson, N. E. Kinetics and mechanism for the alkaline homogeneous hydrolysis of 1,1,1-trimethylolethane trinitrate. *J. Org. Chem.* **1983**, *48*, 315−321.
(35) Capellos, C.; Fisco, W. J.; Ribaudo, C.; Hogan, V. D.; Campisi, J.; Murphy, F. X.; Castorina, T. C.; Rosenblatt, D. H. Basic hydrolysis of glyceryl nitrate esters. I. 1-glyceryl and 2-glyceryl nitrate esters. *Int. J. Chem. Kinet.* **1982**, *14*, 903−917.
(36) Boschan, R.; Merrow, R. T.; Van Dolah, R. W. The chemistry of nitrate esters. *Chem. Rev.* **1955**, *55*, 485−510.
(37) Koshy, K. M.; Robertson, R. E. The nucleophilic displacement of the nitrate group. 1. The hydrolysis of a series of benzyl nitrates in water. *Can. J. Chem.* **1974**, *52*, 2485−2490.
(38) Wang, D.; Xiao, H.; Li, S. Quantum mechanical and molecular mechanical studies of the hydrolysis of methyl nitrate and the solvent effect. *J. Phys. Org. Chem.* **1992**, *5*, 361−366.
(39) Gaffney, J. S.; Fajer, R.; Senum, G. I.; Lee, J. H. Measurement of the reactivity of OH with methyl nitrate: Implications for prediction of alkyl nitrate-OH reaction rates. *Int. J. Chem. Kinet.* **1986**, *18*, 399−407.
(40) Kames, J.; Schurath, U. Alkyl nitrates and bifunctional nitrates of atmospheric interest: Henry's law constants and their temperature dependencies. *J. Atmos. Chem.* **1992**, *15*, 79−95.
(41) Frisch, M. J.; Trucks, G. W.; Schlegel, H. B.; Scuseria, G. E.; Robb, M. A.; Cheeseman, J. R.; Scalmani, G.; Barone, V.; Petersson, G. A.; Nakatsuji, H.; et al. *Gaussian 16*, Revision B.01; Gaussian, Inc.; Wallingford CT, 2016.
(42) Chen, W.-L.; Hsieh, C.-M.; Yang, L.; Hsu, C.-C.; Lin, S.-T. A Critical Evaluation on the Performance of COSMO-SAC Models for Vapor-Liquid and Liquid-Liquid Equilibrium Predictions Based on Different Quantum Chemical Calculations. *Ind. Eng. Chem. Res.* **2016**, *55*, 9312−9322.
(43) Chai, J.-D.; Head-Gordon, M. Long-range corrected hybrid density functionals with damped atom-atom dispersion corrections. *Phys. Chem. Chem. Phys.* **2008**, *10*, 6615−6620.
(44) Singh, D. K.; Rathke, B.; Kiefer, J.; Materny, A. Molecular structure and interactions in the ionic liquid 1-ethyl-3-methylimidazolium trifluoromethanesulfonate. *J. Phys. Chem. A* **2016**, *120*, 6274−6286.
(45) Weigend, F.; Ahlrichs, R. Balanced basis sets of split valence, triple zeta valence and quadruple zeta valence quality for H to Rn: design and assessment of accuracy. *Phys. Chem. Chem. Phys.* **2005**, *7*, 3297−3305.
(46) Weigend, F. Accurate Coulomb-fitting basis sets for H to Rn. *Phys. Chem. Chem. Phys.* **2006**, *8*, 1057−1065.
(47) Voss, J. M.; Marsh, B. M.; Zhou, J.; Garand, E. Interaction between ionic liquid cation and water: infrared predissociation study of [bmim]+·(H2O)n clusters. *Phys. Chem. Chem. Phys.* **2016**, *18*, 18905−18913.
(48) Smith, B. J.; Marsden, C. J. Conformational preferences of XONO2 systems (X = H, F, Cl, CH3) from ab initio techniques. *J. Comput. Chem.* **1991**, *12*, 565−574.
(49) Cox, A. P.; Waring, S. Microwave spectrum, structure and dipole moment of methyl nitrate. *Trans. Faraday Soc.* **1971**, *67*, 3441−3450.
(50) Bunte, S. W.; Sun, H. Molecular modeling of energetic materials: the parameterization and validation of nitrate esters in the COMPASS force field. *J. Phys. Chem. B* **2000**, *104*, 2477−2489.
(51) Durig, J. R.; Sheehan, T. G. Raman spectra, vibrational assignment, structural parameters and ab initio calculations for ethyl nitrat. *J. Raman Spectrosc.* **1990**, *21*, 635−644.
(52) Arenas, J. F.; Avila, F. J.; Otero, J. C.; Peláez, D.; Soto, J. Approach to the atmospheric chemistry of methyl nitrate and methylperoxy nitrite. Chemical mechanisms of their formation and decomposition reactions in the gas phase. *J. Phys. Chem. A* **2008**, *112*, 249−255.
(53) Soto, J.; Peláez, D.; Otero, J. C.; Avila, F. J.; Arenas, J. F. Photodissociation mechanism of methyl nitrate. A study with the multistate second-order multiconfigurational perturbation theory. *Phys. Chem. Chem. Phys.* **2009**, *11*, 2631−2639.
(54) Scroggin, D. G.; Riveros, J. M.; Wilson, E. B. Microwave spectrum and rotational isomerism of ethyl nitrate. *J. Chem. Phys.* **1974**, *60*, 1376−1385.
(55) Gong, X. D.; Xiao, H. M. Ab initio and density functional methods studies on the conformations and thermodynamic properties of propyl nitrate. *J. Mol. Struct.: THEOCHEM* **2000**, *498*, 181−190.
(56) Marenich, A. V.; Cramer, C. J.; Truhlar, D. G. Universal solvation model based on solute electron density and on a continuum model of the solvent defined by the bulk dielectric constant and atomic surface tensions. *J. Phys. Chem. B* **2009**, *113*, 6378−6396.

(57) Kříž, K.; Řezáč, J. Reparametrization of the COSMO solvent model for semiempirical methods PM6 and PM7. *J. Chem. Inf. Model.* **2019**, *59*, 229−235.
(58) Fehér, P. P.; Stirling, A. Assessment of reactivities with explicit and implicit solvent models: QM/MM and gas-phase evaluation of three different Ag-catalysed furan ring formation routes. *New J. Chem.* **2019**, *43*, 15706−15713.
(59) Mahmoudzadeh, G.; Ghiasi, R.; Pasdar, H. Solvent Influence on Structure and Electronic Properties of Si2Me4: A Computational Investigation Using PCM-SCRF Method. *Russ. J. Phys. Chem. A* **2019**, *93*, 2244−2249.
(60) Mera-Adasme, R.; Rezende, M. C.; Domínguez, M. On the physical-chemical nature of solvent polarizability and dipolarity. *Spectrochim. Acta, Part A* **2020**, *229*, 118008−118013.
(61) Shenderovich, I. G.; Denisov, G. S. Adduct under Field-A Qualitative Approach to Account for Solvent Effect on Hydrogen Bonding. *Molecules* **2020**, *25*, 436.
(62) Silva, N. M.; Deglmann, P.; Pliego, J. R., Jr CMIRS solvation model for methanol: parametrization, testing, and comparison with SMD, SM8, and COSMO-RS. *J. Phys. Chem. B* **2016**, *120*, 12660−12668.
(63) Xu, L.; Coote, M. L. Methods to improve the calculations of solvation model density solvation free energies and associated aqueous pKa values: comparison between choosing an optimal theoretical level, solute cavity scaling, and using explicit solvent molecules. *J. Phys. Chem. A* **2019**, *123*, 7430−7438.
(64) Chen, J.; Shao, Y.; Ho, J. Are explicit solvent models more accurate than implicit solvent models? A case study on the Menschutkin reaction. *J. Phys. Chem. A* **2019**, *123*, 5580−5589.
(65) Miguel, E. L. M.; Santos, C. I. L.; Silva, C. M.; Pliego, J. R., Jr How accurate is the SMD model for predicting free energy barriers for nucleophilic substitution reactions in polar protic and dipolar aprotic solvents? *J. Braz. Chem. Soc.* **2016**, *27*, 2055−2061.
(66) Ostovari, H.; Zahedi, E.; Sarvi, I.; Shiroudi, A. Kinetic and mechanistic insight into the formation of amphetamine using the Leuckart-Wallach reaction and interaction of the drug with GpC·CpG base-pair step of DNA: a DFT study. *Monatsh. Chem.* **2018**, *149*, 1045−1057.
(67) Kubečka, J.; Besel, V.; Kurtén, T.; Myllys, N.; Vehkamäki, H. Configurational sampling of noncovalent (atmospheric) molecular clusters: sulfuric acid and guanidine. *J. Phys. Chem. A* **2019**, *123*, 6022−6033.
(68) Zhang, J.; Dolg, M. ABCluster: the artificial bee colony algorithm for cluster global optimization. *Phys. Chem. Chem. Phys.* **2015**, *17*, 24173−24181.
(69) Zhang, J.; Dolg, M. Global optimization of clusters of rigid molecules using the artificial bee colony algorithm. *Phys. Chem. Chem. Phys.* **2016**, *18*, 3003−3010.
(70) Beckstein, O.; Fourrier, A.; Iorga, B. I. Prediction of hydration free energies for the SAMPL4 diverse set of compounds using molecular dynamics simulations with the OPLS-AA force field. *J. Comput. Aided Mol. Des.* **2014**, *28*, 265−276.
(71) Bannwarth, C.; Ehlert, S.; Grimme, S. GFN2-xTB-An Accurate and Broadly Parametrized Self-Consistent Tight-Binding Quantum Chemical Method with Multipole Electrostatics and Density-Dependent Dispersion Contributions. *J. Chem. Theory Comput.* **2019**, *15*, 1652−1671.
(72) Grimme, S.; Bannwarth, C.; Shushkov, P. A Robust and Accurate Tight-Binding Quantum Chemical Method for Structures, Vibrational Frequencies, and Noncovalent Interactions of Large Molecular Systems Parametrized for All spd-Block Elements (Z = 1-86). *J. Chem. Theory Comput.* **2017**, *13*, 1989−2009.
(73) Fukui, K. The path of chemical reactions - the IRC approach. *Acc. Chem. Res.* **1981**, *14*, 363−368.
(74) *Theory and Applications of Computational Chemistry: The First Forty Years*; Dykstra, C., Frenking, G., Kim, K., Scuseria, G., Eds.; Elsevier, 2011.
(75) Scuseria, G. E.; Schaefer, H. F., III Is coupled cluster singles and doubles (CCSD) more computationally intensive than quadratic configuration interaction (QCISD)? *J. Chem. Phys.* **1989**, *90*, 3700−3703.
(76) Pople, J. A.; Head-Gordon, M.; Raghavachari, K. Quadratic configuration interaction. A general technique for determining electron correlation energies. *J. Chem. Phys.* **1987**, *87*, 5968−5975.
(77) Dunning, T. H., Jr Gaussian basis sets for use in correlated molecular calculations. I. The atoms boron through neon and hydrogen. *J. Chem. Phys.* **1989**, *90*, 1007−1023.
(78) Neese, F. The ORCA program system. *Wiley Interdiscip. Rev.: Comput. Mol. Sci.* **2012**, *2*, 73−78.
(79) Zhou, H.-X. Rate theories for biologists. *Q. Rev. Biophys.* **2010**, *43*, 219−293.
(80) Roa, R.; Kim, W. K.; Kanduč, M.; Dzubiella, J.; Angioletti-Uberti, S. Catalyzed Bimolecular Reactions in Responsive Nanoreactors. *ACS Catal.* **2017**, *7*, 5604−5611.
(81) Åqvist, J.; Kazemi, M.; Isaksen, G. V.; Brandsdal, B. O. Entropy and enzyme catalysis. *Acc. Chem. Res.* **2017**, *50*, 199−207.
(82) Bao, J. L.; Truhlar, D. G. Variational transition state theory: theoretical framework and recent developments. *Chem. Soc. Rev.* **2017**, *46*, 7548−7596.
(83) Sun, J.; Wei, B.; Mei, Q.; An, Z.; Wang, X.; Han, D.; Xie, J.; Zhan, J.; Zhang, Q.; Wang, W.; et al. Theoretical investigation on the degradation of dibutyl phthalate initiated by OH and SO4·- in aqueous solution: Mechanism, kinetics and ecotoxicity assessment. *Chem. Eng. J.* **2020**, *382*, 122791−122800.
(84) Eckart, C. The penetration of a potential barrier by electrons. *Phys. Rev.* **1930**, *35*, 1303−1309.
(85) Shavitt, I. A Calculation of the Rates of the Ortho-Para Conversions and Isotope Exchanges in Hydrogen. *J. Chem. Phys.* **1959**, *31*, 1359−1367.
(86) Hermans, I.; Vereecken, L.; Jacobs, P. A.; Peeters, J. Mechanism of the catalytic oxidation of hydrocarbons by N-hydroxyphthalimide: a theoretical study. *Chem. Commun.* **2004**, 1140−1141.
(87) Sarkar, S.; Mallick, S.; Deepak, D.; Kumar, P.; Bandyopadhyay, B. Isomerization of methoxy radical in the troposphere: competition between acidic, neutral and basic catalysts. *Phys. Chem. Chem. Phys.* **2017**, *19*, 27848−27858.
(88) Lee, S.; Karplus, M. Kinetics of diffusion-influenced bimolecular reactions in solution. I. General formalism and relaxation kinetics of fast reversible reactions. *J. Chem. Phys.* **1987**, *86*, 1883−1903.
(89) Miller, C. C. The Stokes-Einstein law for diffusion in solution. *Proc. R. Soc. London, Ser. A* **1924**, *106*, 724−749.
(90) Galano, A.; Alvarez-Idaboy, J. R. Kinetics of radical-molecule reactions in aqueous solution: A benchmark study of the performance of density functional methods. *J. Comput. Chem.* **2014**, *35*, 2019−2026.
(91) Varela, J. A.; Vázquez, S. A.; Martínez-Núñez, E. An automated method to find reaction mechanisms and solve the kinetics in organometallic catalysis. *Chem. Sci.* **2017**, *8*, 3843−3851.
(92) Wagner, W.; Kretzschmar, H.-J. IAPWS industrial formulation 1997 for the thermodynamic properties of water and steam. *International Steam Tables: Properties of Water and Steam Based on the Industrial Formulation IAPWS-IF97*; Springer, 2008, pp 7−150.
(93) Shi, Q.; Zhang, W.; Ji, Y.; Wang, J.; Qin, D.; Chen, J.; Gao, Y.; Li, G.; An, T. Enhanced uptake of glyoxal at the acidic nanoparticle interface: implications for secondary organic aerosol formation. *Environ. Sci.: Nano* **2020**, *7*, 1126−1135.
(94) Tsui, W. G.; Woo, J. L.; McNeill, V. F. Impact of aerosol-cloud cycling on aqueous secondary organic aerosol formation. *Atmosphere* **2019**, *10*, 666.
(95) Herrmann, H.; Schaefer, T.; Tilgner, A.; Styler, S. A.; Weller, C.; Teich, M.; Otto, T. Tropospheric aqueous-phase chemistry: kinetics, mechanisms, and its coupling to a changing gas phase. *Chem. Rev.* **2015**, *115*, 4259−4334.
(96) McKinley-McKee, J. S.; Moelwyn-Hughes, E. A. The kinetics of the hydrolysis of methyl nitrate and of methyl acetate in aqueous solution. *Trans. Faraday Soc.* **1952**, *48*, 247−253.